Synthesis and Characterization of $Ba_xSr_{1-x}Fe_{0.8}Co_{0.2}O_{3-\delta}(0\leq x\leq 1)$ Ceramic membranes

By

SANDEEP KUMAR SINGH

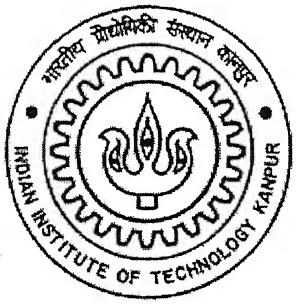

Material Science Programme
Indian Institute of Technology, Kanpur

December, 2004

Synthesis and Characterization of $Ba_xSr_{1-x}Fe_{0.8}Co_{0.2}O_{3-\delta}(0\leq x\leq 1)$ Ceramic membranes

A Thesis submitted
In Partial Fulfillment of the Requirements
For the Degree of

MASTER OF TECHNOLOGY

By

SANDEEP KUMAR SINGH

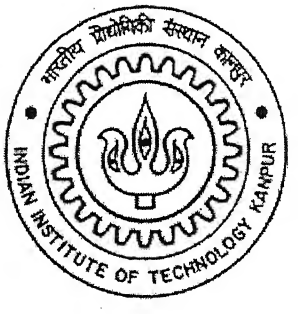

Material Science Programme
Indian Institute of Technology, Kanpur
December, 2004

TO

My Parents
&
My Dear Wife
Roli

CERTIFICATE

This is to certify that the research work contained in the M.Tech. thesis entitled "***Synthesis and Characterization of $Ba_xSr_{1-x}Fe_{0.8}Co_{0.2}O_{3-\delta}(0\leq x\leq 1)$ Ceramic membranes*** " by Mr. Sandeep Kumar Singh has been carried out under my supervision and this work has not been submitted elsewhere for a degree.

Jitendra Kumar

(Jitendra Kumar)
Professor
Material Science Programme
Indian Institute of Technology,
Kanpur 208016

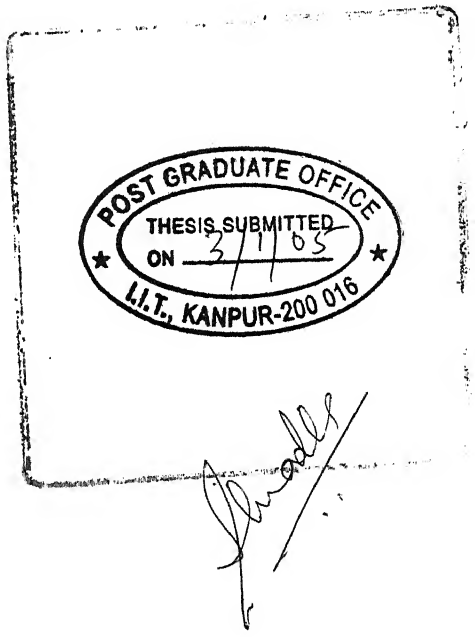

Acknowledgement

I feel pleasure in expressing my sincere gratitude to Prof. Jitendra Kumar for his invaluable guidance, keen interest, needed cooperation and continuous encouragement during the course of this investigation.

I appreciate Thapaji for his timely help during my experimental work. I give special thanks to Uma shankarji, Sharmaji, Shiv Kumarji, Prasad ji and Paul for their constant help throughout the experiments.

It is beyond my words to thank my dear family for the opportunity they have provided me and for the love and affection bestowed on me.

Sandeep Kumar Singh

Contents

Figure	List of Figures	Page.
Fig 1.1	Modes of operation of solid electrolytes for the separation of oxygen	4
Fig 1.2	Types of mixed ionic-electronic conducting dense membranes	5
Fig 1.3	Schematic survey of fluxes and reactions in mixed-conducting membrane reactors	7
Fig 2.1	Flow chart of the combined citrate and EDTA complexing method	13
Fig 2.2	The pulse Chemisorb 2705	16
Fig 2.3	Peak data from the sample	17
Fig 3.1	Weight versus Temperature and –dw/dT versus temperature plot for $Ba_xSr_{1-x}Fe_{0.8}Co_{0.2}O_{3-\delta}$	19-22
Fig 3.2	XRD pattern of $Ba_xSr_{1-x}Fe_{0.8}Co_{0.2}O_{3-\delta}$ for $(0\leq x\leq 1)$	24-27
Fig 3.2.1	Schematic diagram of ideal perovskite structure	29
Fig 3.2.2	Barium content versus lattice parameter	30
Fig 3.3.1	Hysteresis curves of $Ba_xSr_{1-x}Fe_{0.8}Co_{0.2}O_{3-\delta}$	33
Fig 3.3.2	Hysteresis parameters versus compositions	34
Fig 3.3.3	Magnetization versus Temperature	35
Fig 3.4	Oxygen temperature-programmed desorption curves of $Ba_xSr_{1-x}Fe_{0.8}Co_{0.2}O_{3-\delta}$	37
Fig 3.5	XRD pattern after O_2-TPD experiment	38

Abstract

The compounds of compositions $Ba_xSr_{1-x}Fe_{0.8}Co_{0.2}O_{3-\delta}$ ($0 \leq x \leq 1$; in the interval of x=0.2) have been synthesized using a combined citrate-EDTA complexing method and characterized with regard to their thermal stability, phase (s), magnetic properties and oxygen desorption to understand the effect of partial substitution of strontium with barium and to ascertain their suitability as ceramic membrane for oxygen separation application at high temperatures. It is shown that weight loss of the resulting raw powder takes place upto 900^0C; the overall weight loss being about 75%. The compounds, however, remain stable above 820^0C for x=0.6 and 900^0C for all other compositions. X-ray diffraction studies revealed the crystal structure of compounds as cubic (perovskite type) for all compositions except x=1.0 and the progressive increase in lattice parameter with increase in barium content; the value being in the range (3.888-4.052) ± 0.004 Å. $BaFe_{0.8}Co_{0.2}O_{3-\delta}$ compound depicts an hexagonal structure with a=5.889 Å, c=4.653 Å (the accuracy being ± 0.004 Å). Barium substitution is found to lower the overall magnetization and increase the coercivity value of system. Further, the Curie temperature of $SrFe_{0.8}Co_{0.2}O_{3-\delta}$ and $Ba_{0.5}Sr_{0.5}Fe_{0.8}Co_{0.2}O_{3-\delta}$ compound turns to be 575^0 and 600^0C , respectively (the later being more stable magnetically). It is believed that the partial substitution of strontium with barium in $SrFe_{0.8}Co_{0.2}O_{3-\delta}$ facilitates the oxidation of Co^{3+} to Co^{4+} and Fe^{3+} to Fe^{4+}. The optimum working temperature of the compounds as ceramic membrane for oxygen separation application is shown to be 850^0 and 915^0C for $SrFe_{0.8}Co_{0.2}O_{3-\delta}$ and $Ba_{0.5}Sr_{0.5}Fe_{0.8}Co_{0.2}O_{3-\delta}$, respectively.

Chapter 1

1.1 Introduction

Ceramic membranes have drawn attention of academia as well as industries in the recent past due to their application as separators and inherent stability in extreme operating conditions (e.g., high temperature and large pressure gradient). Also they withstand attack from chemically active mixture. Unlike organic membrane, these are invulnerable to microbial degradation and their service life is three to five times larger. A recent report showed that almost half of the earth's volume is composed of perovskite-type compounds, with the formula ABO_3,as the high-pressure phase of $(Mg,Fe)SiO_3$ and $CaSiO_3$. Their structure can be described be a cubic unit cell which contain an A-ion at the center of a cube, B-ions at the corners and oxygen ions at the centre of cell edge (termed as A-type cell). Alternately B-ions lie at the centre with A-ions at the corners and oxygen ons at the face-centred positions of a cube (called as B-type cell). Various combinations of ions provided that the charge balance holds among the component ions and the ionic radii of A-,B-, and O-site ions (r_A,r_B, and r_O,respectively) satisfy the condition $0.71<t<1$, where the tolerance factor(t) is defined by

$$t = (r_A + r_O)/ [2^{1/2} (r_B + r_O)] \qquad (1)$$

Perovskite-type ABO_3 compounds with various properties can be insulators, dielectrics, magnetic materials, electronic conductors, ionic conductors, mixed conductors, and superconductors. Some are chemically quite active and so are good catalysts. In general, the nature of a perovskite-type compound is determined by its B-site ions. For example, high conductivity compounds usually have B-site ions of mixed-valence state, while insulators generally have fixed-

valence B-site ions. Their properties are quite sensitive to the oxygen deficiency and A-site occupancy. Various functional properties of perovskite-type oxide (ABO_3) can be easily modified by the total or partial replacement of cations at A- and/or B-sites. When the B-ions have a mixed-valence state (e.g., transition metals), the partial substitution of A-site cations by other metal ions with lower valency usually causes the formation of oxygen vacancies and a change in the valence state of the B-ions in order to maintain the charge neutrality [1]. With trivalent transition metal ions in the B-site and a trivalent rare earth in the A-position, the compounds exhibits p-type conduction with majority and minority nonstoichiometric defects as cation and oxygen vacancies, respectively. However, the mobility of oxygen is greater than that of cations. To enhance the ionic conductivity it is essential to increase of the oxygen vacancy concentration somehow. One way for ensuring this is by substitution of acceptors at the A- or B-sites, on replacing B-ions with smaller but lower valence ions [2-6]. Perovskite type-oxides are characterized by large departures from ideal stoichiometry ABO_3. This situation prevails when the aliovalent cations are used for the substitution or redox process occurs in the presence of transition metal atoms, capable of assuming different oxidation states. The oxygen vacancies tend to disorder at elevated temperatures, maximizing their configurational entropy, and so become highly mobile [7]. The mixed oxides, of the type $A_x A'_{1-x} B_y B'_{1-y} O_{3-\delta}$ (A = La; A' = Ba,Sr,Ca; B= Cr,Fe,Co,Mn; B'= Ni,Cu) show a high ionic conductivity as well as electronic conductivity due to the oxygen vacancies and mixed-valence state respectively. Some of these perovskites exhibit oxygen permeability 1 to 2 orders of magnitude higher than conventional stabilized zirconia and so possess potential application as permeation membranes for separation of oxygen from air without the use of any external electrical circuit. In fact, these provide a clean, efficient and economical means of producing oxygen from air or gas mixtures. Other applications of ABO_3 type oxides include partial oxidation of methane to syngas [8-12], oxidative couplers to value-added products, such as ethane [13-15].

1.2 Oxygen separation methods

At present oxygen is produced on industrial scale mainly by cryogenic distillation of air. This is a very energy intensive process and economic operation is possible only on a large scale. An alternative method is pressure swing adsorption, where nitrogen from compressed air is adsorbed preferentially on active carbon or a zeolite. After removal of the oxygen-enriched air, the pressure is reduced to desorb the nitrogen. This can be operated economically at smaller scale but has the disadvantage of being a discontinuous process. A relatively new development is the dense ceramic membranes which can exclusively separate oxygen from air at high temperatures [16]. In future, these membranes may possibly be applied in small scale units for the production of pure oxygen, in the field of chemical processing, such as the partial oxidation of hydrocarbons.

The ability for separation is based on the existence of high concentration of vacant oxygen crystallographic sites in the ceramic membrane. At elevated temperatures the oxygen anions become mobile and their diffusion occurs via neighboring oxygen vacancies. In a number of cases, sufficient internal space exists to allow oxygen anions to occupy interstitial sites, which may contribute further to the oxygen ion conductivity. Two types of dense membranes can be distinguished as the *solid electrolytes* and the *mixed ionic-electronic conductors*. The solid electrolytes are pure oxygen ion conducting materials. In order to operate as an oxygen separation membrane, electrodes are deposited on both sides, and external wiring is attached. At the triple phase boundary line between the oxide, the electrode and the gas phase, oxygen may be incorporated into or released from the structure following the net exchange reaction $O_2 + 4e^- \rightarrow 2O^{2-}$.

A solid electrolyte membrane can be operated in two different modes, as depicted schematically in Figure 1.1 [17, 18]. The primary purpose of solid oxide fuel cell mode (Fig 1.1a) is for the generation of electrical energy. The cathode is exposed to air. An oxygen-consuming chemical reaction takes place in the anode compartment, causing thereby a local decrease in the thermodynamic potential of oxygen. The driving force for oxygen transport is the pressure gradient across

the membrane. In principle, useful chemicals can be co-generated next to electricity if a proper choice is made for the oxidation reaction in the anode compartment.

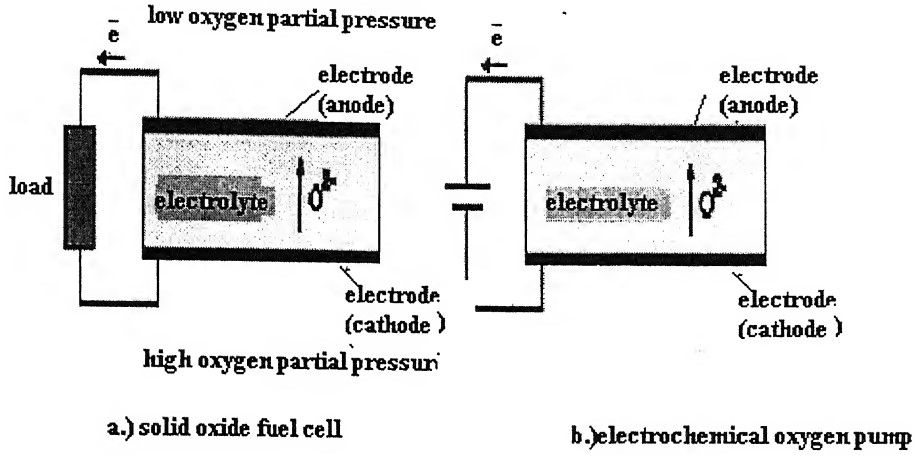

Fig.1.1 Modes of operation of solid electrolytes for the separation of oxygen

Figure 1.1b shows the electrical oxygen pumping mode. The driving force for O_2-transport through the electrolyte is an externally imposed electrical potential difference between the anode and cathode. In most cases, a chemical reaction where rate is affected directly by the supply or removal of oxygen is carried out in one of the compartments. In a number of cases it has been observed that the catalytic activity of the electrode itself is altered strongly upon electrochemical pumping of oxygen [19]. Commonly known solid electrolytes are δ-Bi_2O_3 and yuttria-stabilized zirconia (YSZ). The δ-cubic phase of Bi_2O_3 is the best oxygen ion conductor known. In this, 25% of the crystallographic sites of oxygen are vacant. The high mobility of oxygen is due to the nature of bismuth [20]. The occurrence of oxygen vacancies in stabilized zirconia is due to the partial substitution of Zr^{4+} by cations with a lower valency (e.g.; Y^{3+}, Ca^{2+} or Mg^{2+}). In order to compensate for the lack of positive charge caused by substitution, oxygen vacancies get created. For instance, Yttrium and calcium-stabilized zirconia assume composition $Zr_{1-x}Y_xO_{2-1/x}$ and $Zr_{1-x}Ca_xO_{2-x}$, respectively. Stabilized zirconia membranes found to be thermally, mechanically and chemically stable.

An alternative to solid electrolytes are the mixed ionic-electronic conductors. Apart from ionic conductivity these materials exhibit significant electronic conductivity and provide an internal short-circuit. For this reason, these membranes do not need electrodes and an external circuit for the separation of oxygen. When a mixed conducting membrane is placed in an oxygen partial pressure gradient, anions permeate from the high to the low partial pressure side, while overall charge neutrality is maintained by a counterbalancing flux of electrons (and/or holes), as depicted schematically in Figure 1.2a.

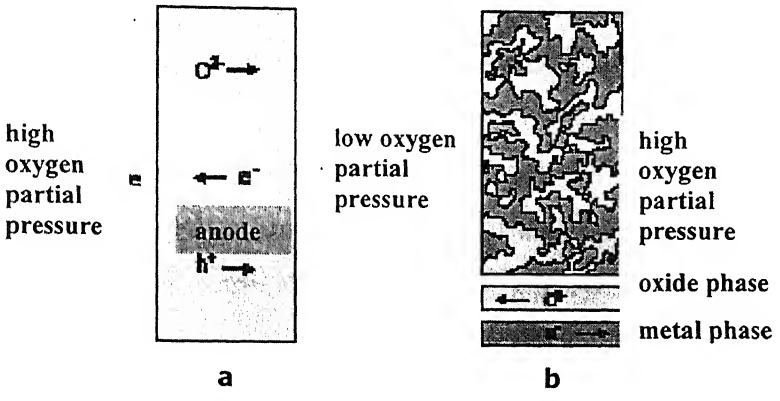

Fig.1.2 Types of mixed ionic-electronic conducting dense membranes. a) single phase membrane; b) dual phase composite membrane

Both calcium-stabilized zirconia [21] and erbium-stabilized bismuth oxide ($Bi_{1.5}Er_{0.5}O_3$) have been used as mixed conducting membranes in oxygen pressure gradients [22]. But it is demonstrated that the chemical diffusion of O^{2-} in them gets limited by the electronic conductivity. Attempts have been made to increase the concentration of electronic charge carriers in YSZ and bismuth oxide by partial substitution of zirconium with multivalent elements, e.g., cerium ($Ce^{4+} + e^- \rightarrow Ce^{3+}$) [23] and terbium ($Tb^{4+} + e^- \rightarrow Tb^{3+}$) [24,25], and thereby influencing the concentration of oxygen vacancies as well. Although the oxygen semi-permeability could be enhanced by these substitutions, yet the observed fluxes remained relatively low.

Teraoka et al. [26] reported a series of perovskite-type $LaMO_3$ compounds (M=C0 and/or Fe), with partial substitution of La^{3+} by Sr^{2+} and compositions La_{1-}

$_xSr_xCo_{1-y}Fe_y O_{3-\delta}$ (x=0-1, y=0-1) δ denotes the average number of vacant oxygen sites per unit cell determining the level of nonstoichiometry. In this class of materials, charge compensation for the substituted aliovalent Sr-cations involves not only the creation of oxygen vacancies but also the oxidation of a fraction of M^{3+} to M^{4+}. This leads to high concentration of ionic and electronic charge carriers at elevated temperatures (>700°C) [27, 28]. In fact the oxygen semi-permeability is found to increase with increase of the strontium content. The influence of cation substitution in compounds $La_{0.6}A_{0.4}Co_{0.8}Fe_{0.2}O_{3-\delta}$ (A= Na, Ca, Ba, Sr) and $La_{0.6}$ $M_{0.4}Co_{0.8}Fe_{0.2}O_{3-\delta}$ (M=Fe, Co, Ni, Cu) is reported in later studies [29,30]. Apart from fast oxygen diffusion, mixed-conducting perovskite-type oxides exhibit a significant exchange of oxygen with the ambient contributing further to the oxygen flux through these materials. [31, 32]

For oxygen separation from air, cobalt-rich compounds with high concentration of aliovalent substitution appear to be most promising, because they combine high oxygen semi-permeability with chemical stability at elevated temperatures. The systems studied include $SrCo_{0.8}M_{0.2}O_{3-\delta}$ (M=Cr, Fe, Co, Cu) [33,34], $SrCo_{1-x}M_xO_{3-\delta}$ (x=0 - 0.5, M=Ti, Cr, Mn, Fe, Ni, Cu) [35,36], $SrCo_{1-x-y}Fe_xCu_yO_{3-\delta}$ (x=0 - 0.5, y=0 - 0.3) [36], $Ln_{1-x}M_xCoO_{3-\delta}$ (x=0 - 0.9, Ln=La, Pr, Nd; M=Sr, Ca, Bi, Pb) [36-39], $Y_{0.05}BaCo_{0.95}O_{3-\delta}$ [40], $_{0.10}Ba_{0.90}CoO_{3-\delta}$ [40] and $La_{1-x}M_xCo_{1-y}Fe_yO_{3-\delta}$ (M=Sr, Ba, Ca) [41,42]. The oxygen semi-permeability of a number of compounds containing no cobalt e.g., $La_{1-x}Sr_xFeO_{3-\delta}$ (x=0.1, 0.2), $La_{1-x}Ca_xCrO_{3-\delta}$ and $CaTi_{1-x}M_xO_{3-\delta}$ (M=Fe, Co, Ni) is found to be significantly lower than for the cobalt -containing perovskites.[43-46]

Mazanec et al [47] proposed another type of dense membrane with two percolative phases involving ionic and electronic conductivity, respectively (Fig 1.2b). While the transport of oxygen occurs through the ionic conducting phase, the counter flux of electrons takes place through the electronic conducting phase. More recently, cermet membranes based on bismuth oxide, with compositions $Bi_{1.5}Y_{0.5}O_3$-$Ag_{0.7}Pd_{0.3}$, $Bi_{1.5}Y_{0.5}O_3$-Ag, $Bi_{1.5}Er_{0.5}O_3$-Ag and $Bi_{1.5}Er_{0.5}O_3$-Au have been reported [48-49].

1.3 Membrane reactors

Membranes reactors are essentially used in oxidation processes. The major advantage lies in their ability to perform reaction and separation together in a single step and supply oxygen in a controlled manner. For instance, partial oxidation of methane to syngas, ($CH_4+½O_2 \rightarrow CO+2H_2$) requires the supply of pure oxygen as the oxidant. The use of mixed conducting membrane reactors is attractive proposition as both air separation and methane conversion may be achieved in a single step without having a separate-oxygen plant (Figure 1.3). Also the electrochemically supplied O^{2-} is reported to perform better than molecular oxygen in terms of selectivities or conversions [50].

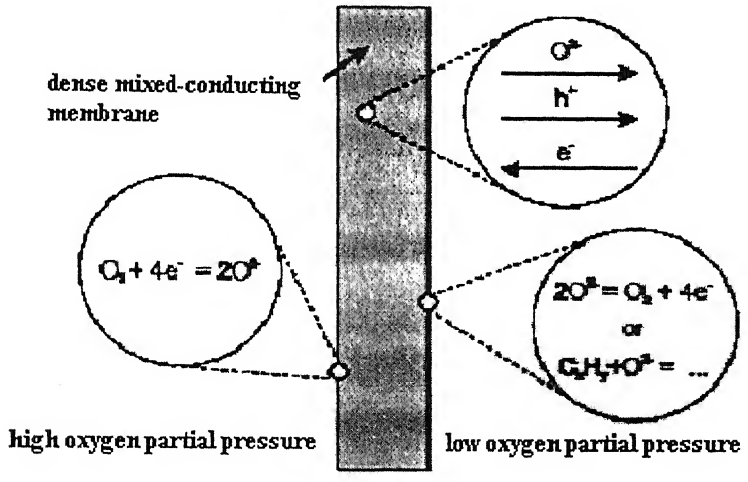

Fig 1.3 Schematic survey of fluxes and reactions in mixed-conducting membrane reactors.

The membrane reactor has been used for thermal splitting of water $H_2O \rightarrow H_2+½O_2$ based on calcium-stabilized zirconia (CSZ) [37,38], thermal decomposition of carbon dioxide $CO_2 \rightarrow CO+½O_2$, [54, 55].

Oxidative coupling of methane to C_2 hydrocarbons (ethane, ethane) has been reported on $BaCe_{0.8}Gd_{0.2}O_{3-\delta}$ membranes at 900°C [57]. The tubes made of $SrCo_{0.8}Fe_{0.2}O_{3-\delta}$ and $La_{0.2}Sr_{0.8}Fe_{0.6}Co_{0.4}O_{3-\delta}$ membranes have been used for the

production of syngas at 900°C[59]. The membranes showed a high catalytic activity to total combustion of methane. Upon introducing an Rh-based catalyst in the reaction compartment, syngas was produced with 90% selectivity to CO and H_2 at a methane conversion of 97%. Direct conversion of methane to syngas with 100% selectivity to CO was reported in a tubular $CaCo_{0.8}Fe_{0.2}O_{3-\delta}$ membrane reactor at 750°C [60].Two-dimensional model calculations of syngas production employing $SrCo_{0.8}Fe_{0.2}O_{3-\delta}$ tubes have shown that the heat generation per unit r volume remains low due to the gradual supply of oxygen along the length of the reactor, thus preventing thermal runaway[62].

1.4 Oxygen permeation transport parameters

There are two basic transport processes defined for oxygen in a ceramic membrane with oxygen partial pressure gradient under the steady state condition: (i) coupled diffusion of oxygen ions and electrons in bulk and (ii) exchange of oxygen at the interfaces.

1.4.1 Coupled diffusion of ionic and electronic species

When the oxygen transport in a membrane is at steady state, there is no net charge current. This relates the fluxes J_i of species i with electrical charge z_i as

$$\sum_{i=1}^{n} Z_i J_i = 0 \qquad (1.1)$$

Limiting the discussion to one-dimensional diffusion in direction x, the flux of a species can be described by [63]

$$J_i = -\frac{\sigma_i}{Z_i^2 F^2} \cdot \frac{\partial \eta_i}{\partial X}, \qquad (1.2)$$

where σ_i is the electrical conductivity of the species, F the Faraday constant, and η_i defined as $\eta_i = \mu_i + z_i F\Phi$ (μ_i indicates the chemical potential of species i, and ϕ is the electrical potential).

If the charge-carrying species in the oxide are taken to be oxygen anion O^{2-}, holes h^+ and electrons e^-, chemical quasi-equilibria may be assumed as

$$½O_2 + 2e^- \rightarrow O^{2-} \quad (1.3)$$

$$e^- + h^+ \rightarrow \text{nil} \quad (1.4)$$

between the molecular oxygen and the membrane oxygen, electrons and holes. Combining Eqs. (1.1) and (1.2) the flux of O^{2-} can be written as

$$J_{O2-} = -\frac{\sigma_{o2-}(\sigma_{e-}+\sigma_{h+})}{(\sigma_{o2-}+\sigma_{e-}+\sigma_{h+})Z_{o2-}^2F^2}\left(\frac{\partial\mu_{o2-}}{\partial X} - \frac{Z_{O2-}}{Z_{e-}}\frac{\sigma_{e-}}{\sigma_{e-}+\sigma_{h+}}\frac{\partial\mu_{e-}}{\partial X} - \frac{Z_{O2-}}{Z_{h+}}\frac{\sigma_{h+}}{\sigma_{e-}+\sigma_{h+}}\frac{\partial\mu_{h+}}{\partial X}\right) \quad (1.5)$$

It follows from the quasi-equilibria (1.3) and (1.4) that

$$½\frac{\partial\mu_{O2}}{\partial X} = \frac{\partial\mu_{O2-}}{\partial X} - 2\frac{\partial\mu_{e-}}{\partial X}, \quad (1.6)$$

$$\frac{\partial\mu_{e-}}{\partial X} = -\frac{\partial\mu_{h+}}{\partial X} \quad (1.7)$$

Taking into account that Z_{O2-}=-2, z_{e-}=-1 and z_{h+} =+1, and comparing Eqs. (1.5), (1.6) and (1.7) one obtains

$$J_{O2-} = -\frac{\sigma_{O2-}(\sigma_{e-}+\sigma_{h+})}{8(\sigma_{O2-}+\sigma_{e-}+\sigma_{h+})F^2}\frac{\partial\mu_{O2}}{\partial X} \quad (1.8)$$

If the thickness of the membrane is L and its interfaces are exposed to oxygen at of P'_{O2} and P''_{O2} at higher and lower side, respectively, oxygen chemical potential can be written as

$$\mu_{O2} = \mu_{O2}^0 + RT\ln p_{O2} \quad (1.9)$$

where μ_{O2}^O is the reference chemical potential at temperature T, and R the gas constant. Taking into account that $J_{O2} = 1/2J_{O2-}$, the oxygen flux becomes

$$J_{O2} = \frac{1}{16F^2L}\int\frac{\sigma_{O2-}(\sigma_{e-}+\sigma_{h+})}{\sigma_{O2-}+\sigma_{e-}+\sigma_h+}d\ln p_{O2} \quad (1.10)$$

This is called the Wagner equation, derived originally for the oxide film growth on metals [64]. In the perovskite-type oxides the total electronic conductivity

$(\sigma_{e-} + \sigma_{h+})$ is usually found to be several orders of magnitude larger than the ionic conductivity σ_{O2-} and so the above expression gets simply to

$$J_{O2-} = \frac{1}{16F^2L} \int_{\ln p_{O2}}^{\ln p'_{O2}} \sigma_{O2-} d \ln p_{O2} \qquad (1.11)$$

The ionic conductivity of a species O^{2-} can be described by [48]

$$\sigma_{O2-} = -\frac{Z^2_{O2-} F^2 D_O c_O}{RT}, \qquad (1.12)$$

where D_O is the self-diffusion coefficient of i, and c_O the concentration of charge carriers. Physically, the transport of oxygen ions and vacancies, occur simultaneously but in the opposite direction. This implies that $D_O\ c_O = D_v\ c_v$, where D_V and c_V are the oxygen vacancy diffusion coefficient and concentration of oxygen vacancy, respectively. The diffusional flux can then be expressed as

$$J_{O2-} = \frac{D_v}{4RTV_m L} \int_{\ln P_{O2}}^{\ln p'_{O2}} \delta d \ln P_{O2}, \qquad (1.13)$$

Here it is all oxygen vacancies are mobile and contribute equally to oxygen transport, so that $c_v = \delta / V_m$, *(V_m being* the unit cell volume of perovskite).

1.4.2 Exchange of oxygen at interfaces

The interaction of membrane oxygen and the gas phase at the interface involves a number of steps, each of which may be rate determining [66, 67], e.g., (i) adsorption O_2 $\rightarrow WO_{2,ads}$,(ii) dissociation $O_{2,ads}$ $\rightarrow 2O_{ads}$,(iii) movement of intermediate species on the surface, (iv) charge transfer $O_{ads} \rightarrow O^-_{asd} + h^+ \rightarrow O^{2-}_{ads} + 2h^+$,and (v) incorporation of O^{2-}_{ads} into the membrane interior. In general it is assumed that reduction of O_2 and oxidation of O^{2-} follow the same sequence of steps in reverse directions [50].

The rate of O_2 exchange at the interface in chemical equilibrium J^{ex}_{O2} is related to the surface exchange coefficient k_0 [50] as

$$J_{O2}^{ex} = \frac{1}{4} k_0 c_0 . \qquad (1.14)$$

Here c_O is the concentration of oxygen anions in the oxide at equilibrium.

1.5 Objective of present work

The objective has been to study the effect of partial substitution of strontium with barium in $SrFe_{0.8}Co_{0.2}O_{3-\delta}$ compound. For this, compounds of composition $Ba_xSr_{1-x}Fe_{0.8}Co_{0.2}O_{3-\delta}$ (x=0 ,0.2, 0.4, 0.5, 0.6, 0.8 and 1.0) have been prepared by combined citrate-EDTA complexing method and characterized with regard to their thermal stability, phase(s), magnetic properties(viz., saturation magnetization, Curie temperature, hysteresis loop, etc) and oxygen desorption behaviour to ascertain their suitability as ceramic membrane for oxygen separation application at high temperatures.

Chapter 2

2.1 Experimental Details

In this chapter, the experimental details pertaining to synthesis of ceramic membranes and their characterization by X-ray diffraction(XRD), thermo gravimetric analysis (TGA),magnetic measurements and oxygen temperature programmed desorption(O_2-TPD) are given.

2.1.1 Synthesis of ceramic membrane

In the preparation of a perovskite-type ABO_3 compound, it is important to: (i) adjust the A/B ratio precisely to unity or in appropriate ratios when the A - or B-site ions are partially substituted with other elements, and (ii) make the product homogeneous. To achieve these objectives, efforts have been made to prepare Ceramic membranes of compositions $Ba_xSr_{1-x}Fe_{0.8}Co_{0.2}O_{3-\delta}$ ($0 \leq x \leq 1$; in the interval of x=0.2) by a combined citrate and EDTA complexing method. Its flow diagram is shown in figure 2.1.

The required amount of barium nitrate $Ba(NO_3)_2$ is first dissolved in ethylene diaamine tetra acetic acid-ammonium hydroxide(EDTA-NH_4OH) solution with continuous stirring and heating. The appropriate amounts of strontium nitrate $Sr(NO_3)_2$,cobalt nitrate $Co(NO_3)_2$ and ferrous nitrate $Fe(NO_3)_3$ are then added to the above solution. After stirring for a while, citric acid is introduced in such a way that the mole ratio of EDTA, citric acid and total metal ions becomes 1:1.5:1. At this stage, NH_4OH was added to adjust the pH value to about 6.0. This turns the solution transparent. Both the molar ratio of metal ions to ligand (i.e., citric acid and EDTA) and the pH influence its overall stability. The final solution is subsequently heated around 50-60^{0}C, stirred continuously for about 24 hours, transferred onto the hot plate to remove water and to yield a dark purple gel. Eventually a soft lump is obtained which can be easily powdered. For the case of $SrFe_{0.8}Co_{0.2}O_{3-\delta}$ (i.e. x=0), instead of $Ba(NO_3)_2$, appropriate amount of $Sr(NO_3)_2$ is first dissolved in EDTA-NH_4OH before adding $Co(NO_3)_2$ and $Fe(NO_3)_2$. For ascertaining thermal

stability, weight of the resulting product is monitored with a balance by raising the temperature at the rate of 3^0C per minute in a laboratory made set-up up to 950^0C. Subsequently, different batches of powders have been calcined at 900^0C for 5 hours each. Calcined powder is sieved with 400 mesh for further study. Pellets of diameter 3mm and 10 mm with thickness of 1.8mm have been made by using a special hard steel die (fabricated for the purpose) at a pressure of 2×10^5KN/m^2 and 6×10^5KN/m^2, respectively.

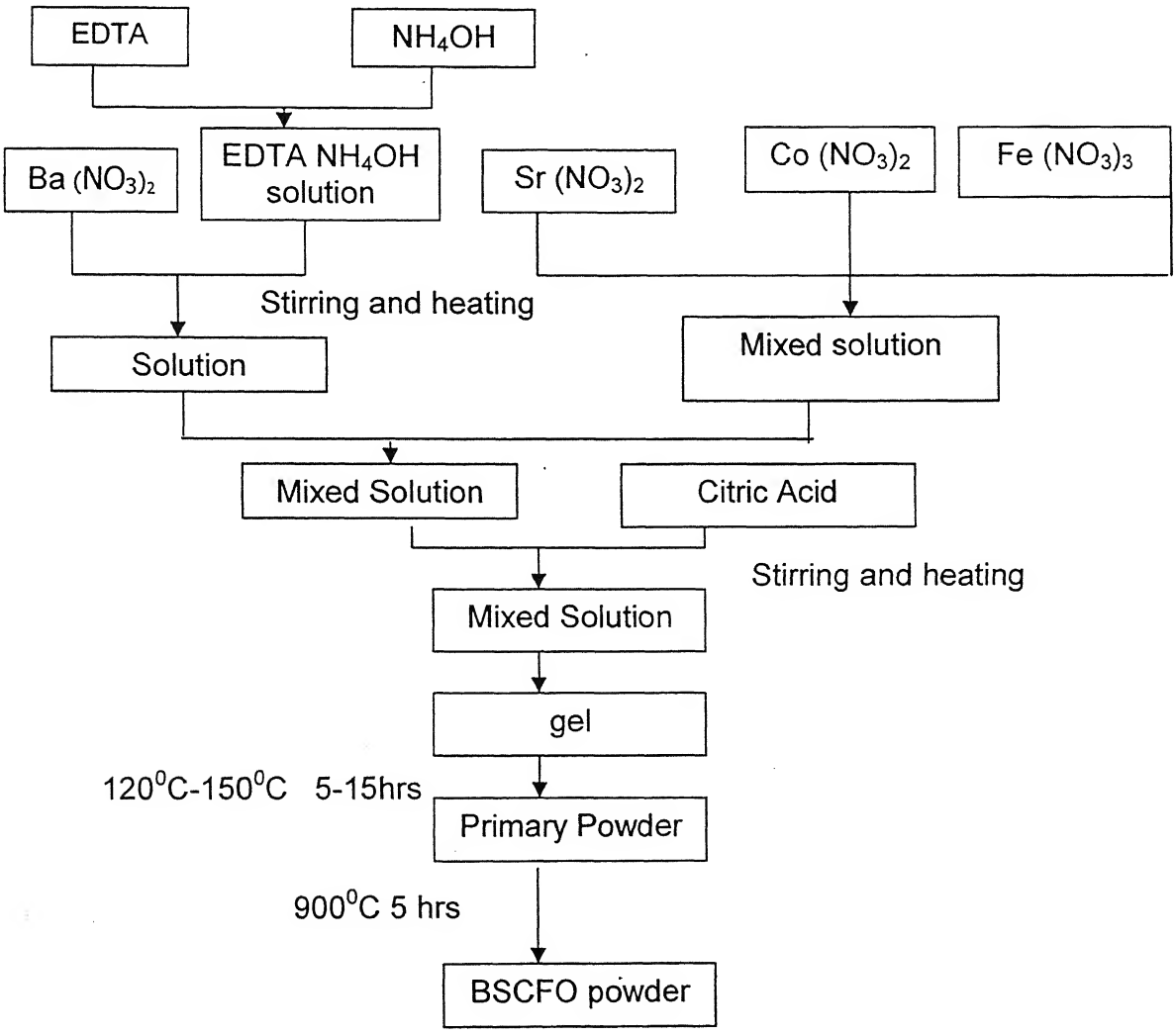

Fig. 2.1. Flow chart of the combined citrate and EDTA complexing method

2.2 Characterization Techniques

2.2.1 Thermogravemetric analysis (TGA)

Thermal analysis is the name applied to a group of techniques having a common operating principle: as a sample is heated or cooled according to a predetermined programme, some physical quantity (e.g., mass, temperature/heat, etc) of the sample is recorded continuously as a function of temperature. The techniques may be classified into three groups depending upon the type of parameter monitored/measured:(i) the absolute value of the sample weight itself, (ii) the temperature difference between the sample and a standard material as a function of time/temperature, and (iii) the rate at which weight-loss or temperature difference is changing with time or temperature or heat supplied to sample or standard with time/temperature. For thermo gravimetric analysis, we developed our own experimental set up using a precision balance model Afcoset ER120A (sensitivity 0.1 mg), an electric cylindrical furnace (maximum achievable temperature 1000^0C) and a programmable temperature controller model Endotherm MPC-500. Sample weight can be as small as 1 mg, but for greater precision and ease of handling, 10-25 mg samples are typically used. The TGA is widely used to measure the loss of volatile components or thermal stability of a sample. The experiments are run with a fixed temperature ramp (e.g., 3 deg/min). The weight losses can be characteristic of material and, where the losses are in discrete steps, the experiment can offer quantitative data on the course of decomposition. The set-up is utilized to determine the nature of the synthesized product for their stability at a heating rate of 3^0 per minute in the temperature range of 25-950^0C.

2.2.2. X-ray Diffraction (XRD)

The XRD patterns of powder samples have been recorded in a Rick Seifert X-ray diffractometer model ISO Debye flux 2002 using a CuKα radiation to ascertain the phase(s) present. For this, powder is packed in a 10 mm diameter circular cavity of aluminium holder which, in turn, is mounted on the sample stage. The diffracted beam is received by a scintillation counter detector held at an angle of 2θ with the transmitted beam(θ being the angle between the sample surface and the incident beam).The rotation movement of the sample and the detector is synchronized such that the incident and diffracted beams always made the same angle(θ) with the sample surface. The X-ray tube has been operated at 30 kV and 20 mA and diffraction pattern recorded at a scanning rate of 3 ^{0}/min in the angle 2θ range of 20-80^0. The time constant was set at 10 seconds and sensitivity is either 5000 or 2000 counts per minutes. XRD pattern is continuously observed on the monitor and data stored in a personal computer for final printing.

2.2.3 Magnetic Measurements

A pellet of 3 mm dia and 1.8 mm thickness is weighed and introduced in the vibrating sample magnetometer(Princeton VSM Model-150)equipped with an electromagnet (Varian model V-2700)capable of providing a maximum magnetic field of ~11.5 kOe. The magnetic moment measurements have been made as a function magnetic field and temperature. A regulated power supply (Networks model NPS 30/5D) is used to provide power to the furnace surrounding the sample and the chamber is evacuated using a pumping system. A chromel-alumel thermocouple is held close to the sample to indicate the temperature. The information derived includes magnetic parameters like saturation magnetization (M_s), coercive field (H_c) and curie temperature (T_c).

2.2.4 Oxygen Temperature-programmed desorption

Oxygen temperature-programmed desorption (O_2-TPD) experiment determines the number, type and strength of active sites on the surface by measuring the amount of gas desorbed at various temperatures. Pulse Chemisorb apparatus model 2705 is shown in Fig 2.2.

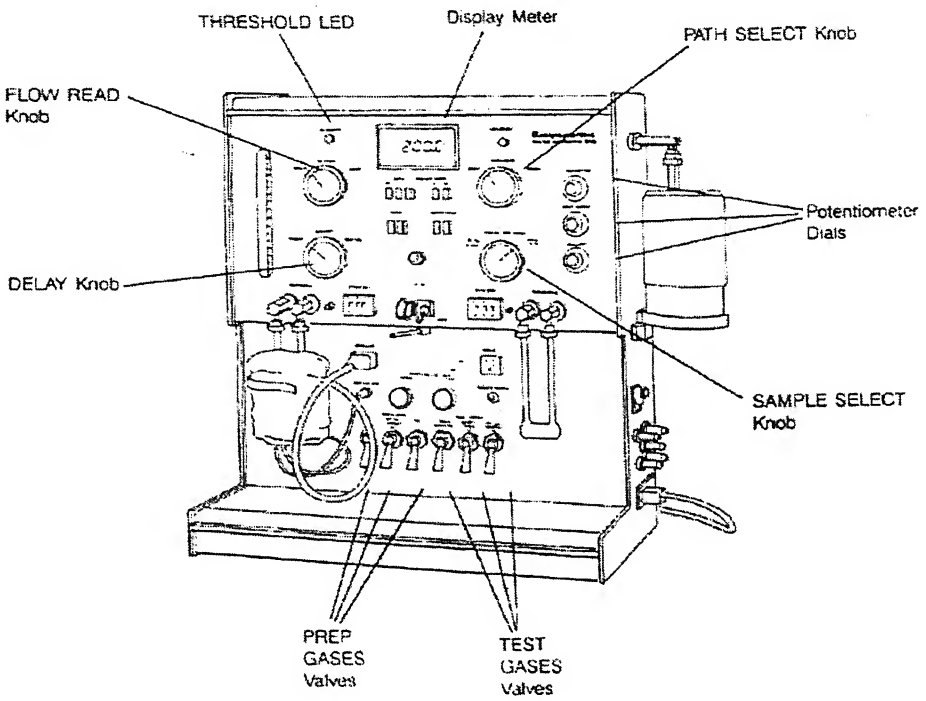

Fig 2.2.The pulse Chemisorb 2705

After the sample has been outgassed or reduced programmed desorption begins by raising the temperature linearly with time while a constant stream of inert carrier gas passes over the sample. At certain temperatures, the desorption occurs from the surface. The desorbed molecules enter the stream of inert carrier gas and are swept to the detector which measures their concentration. The volume of desorbed species combined with the stoichiometry factor and the temperature at which pre-adsorbed species desorb yield the number and strength of active sites. The output data show peaks (as shown in fig.2.3) and

strength of active sites. The output data show peaks (as shown in fig.2.3) and can be reproduced on a chart recorder. The total amount of desorbed oxygen can be calculated from the area under each peak.

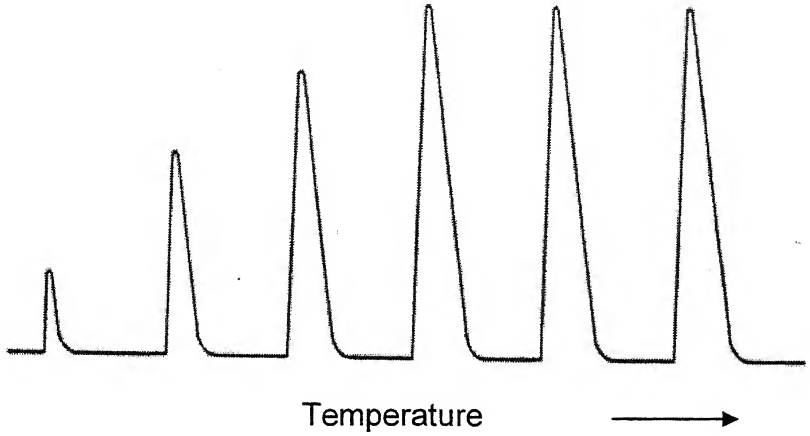

Fig 2.3 Peak data from the sample

A Pulse Chemisorb apparatus model 2705 shown in Fig 2.2 is used for O_2-TPD study of $Ba_xSr_{1-x}Fe_{0.8}Co_{0.2}O_{3-\delta}$. For this, about 0.1 g of sample is loaded in a quartz tube assembly and placed in a single-zone furnace equipped with a temperature controller. Helium has been used as the carrier gas with a flow rate of 30 ml/min. The temperature is increased from 50 to 1000^0C at a rate of 10^0C/min. A thermal conductivity detector (TCD) has been used on line for signal detection with a computer data acquisition system.

Chapter 3

3. Result and discussions

3.1 Thermo gravimetric analysis

As a material decomposes on heating it loses volatile species causing a decrease in weight. Therefore, as successive decomposition reactions occur with increasing temperature, a thermo gravimetric (TG) curve shows a series of sharp weight-losses separated by plateaus of constant weight. However, the weight-loss sometimes does not occur at one temperature, but over a range if processes overlap. In such a situation, a constant-weight plateau does not necessarily occur and the overlap step- like appearance of the ideal TG curve is smoothed out in practice [74].The decomposition temperature regime and fractional weight-loss may be evaluated directly from the TG curve. The maximum rate of weight-loss for each stage is indicated by a point of inflection (P) on the curve. The resolution of complex TG curve is improved by drawing the corresponding differential or derivative thermo-gravimetric curve. The mass versus temperature and –dw/dT versus temperature plots of the synthesized $Ba_xSr_{1-x}Fe_{0.8}Co_{0.2}O_{3-\delta}$ ($0 \leq x \leq 1$) compounds are shown in fig 3.1. The system is stable at 900-950^{0}C for all the compositions. For the some compositions, the stability extends down up to a lower temperature (e.g. 820^{0}C for x=0.6).As barium content is increased beyond x=0.2 the compound exhibit plateau (which means stability) at another temperature range, i.e., 450-650^{0}C. The data derived from the TG curves are summarized in Table 3.1.

Based on the outcome of TG analysis, all the compounds have been annealed at 900^{0}C for 5 hrs for further investigation. This ensured removal of all volatile species contained in the samples at the end of synthesis. The fractional weight of the compound eventually turns to be nearly 0.25 in all cases.

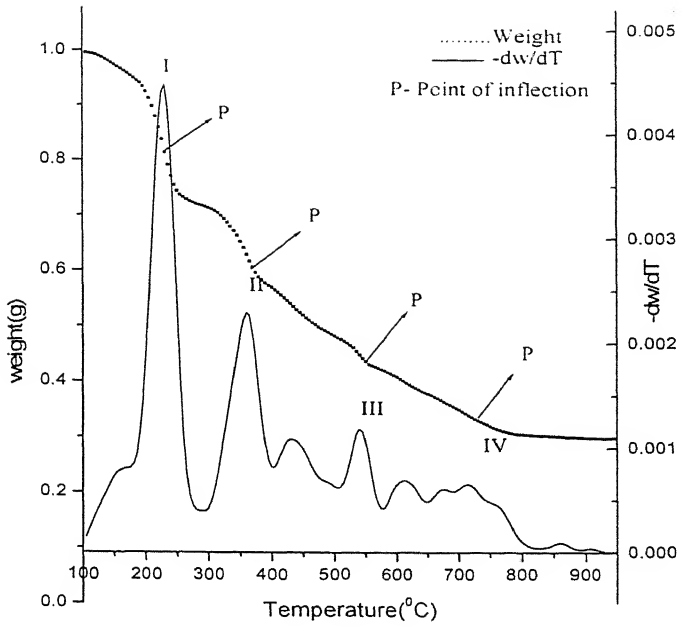

Fig.3.1 (a): Weight versus Temperature and –dw/dT versus Temperature plot for $Ba_xSr_{1-x}Fe_{0.8}Co_{0.2}O_{3-\delta}$ for x=0

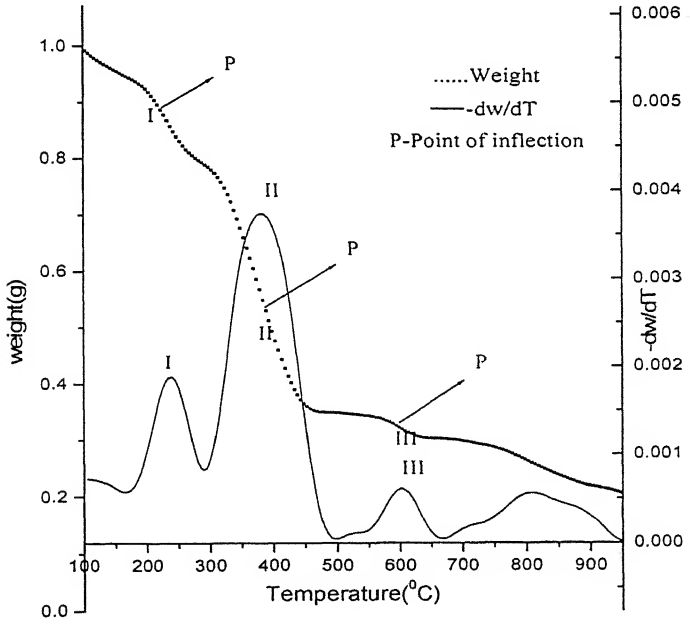

Fig.3.1 (b): Weight versus Temperature and –dw/dT versus Temperature plot for $Ba_xSr_{1-x}Fe_{0.8}Co_{0.2}O_{3-\delta}$ for x=0.2

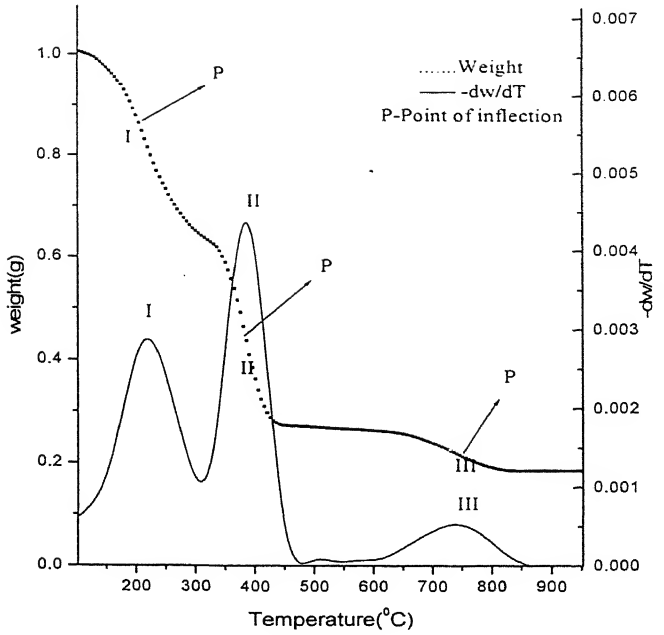

Fig.3.1 (c): Weight versus Temperature and –dw/dT versus Temperature plot for $Ba_xSr_{1-x}Fe_{0.8}Co_{0.2}O_{3-\delta}$ for x=0.4

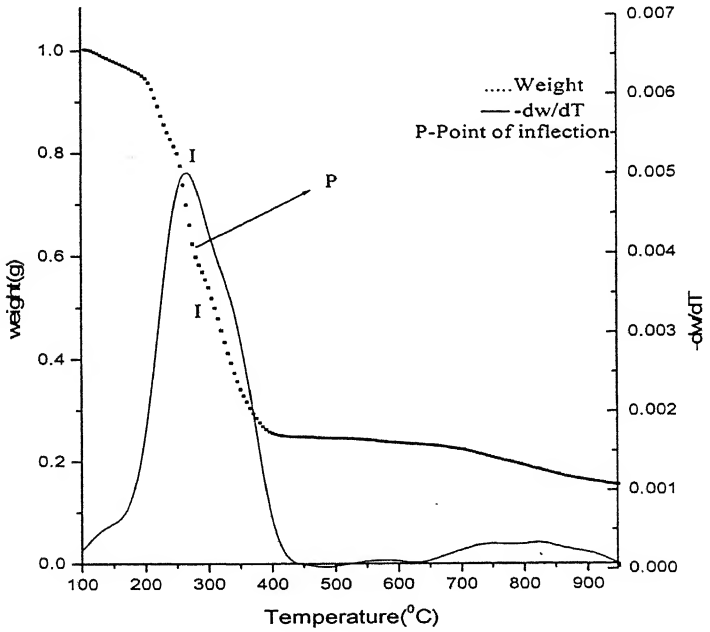

Fig.3.1 (d): Weight versus Temperature and –dw/dT versus Temperature plot for $Ba_xSr_{1-x}Fe_{0.8}Co_{0.2}O_{3-\delta}$ for x=0.5

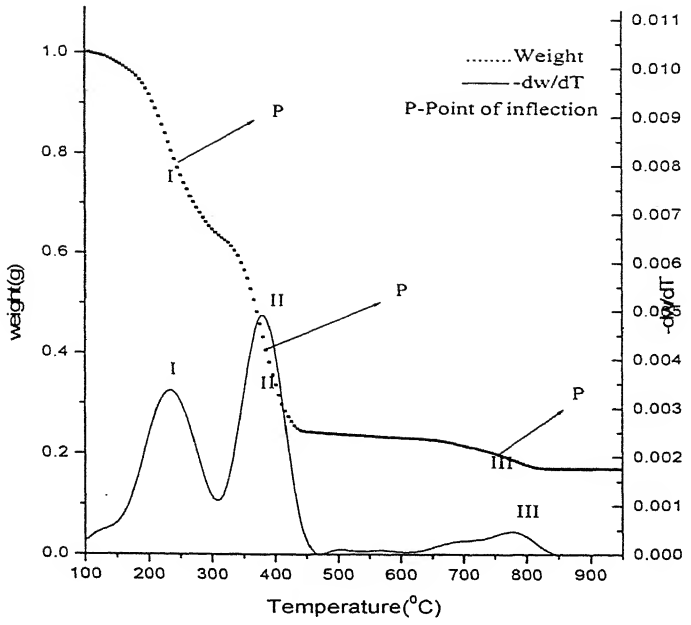

Fig.3.1 (e): Weight versus Temperature and –dw/dT versus Temperature plot for $Ba_xSr_{1-x}Fe_{0.8}Co_{0.2}O_{3-\delta}$ for x=0.6

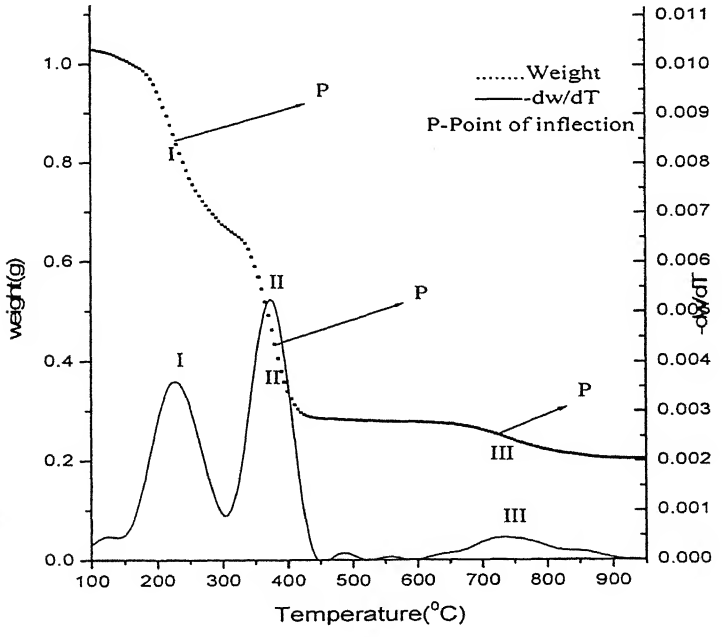

Fig.3.1 (f): Weight versus Temperature and –dw/dT versus Temperature plot for $Ba_xSr_{1-x}Fe_{0.8}Co_{0.2}O_{3-\delta}$ for x=0.8

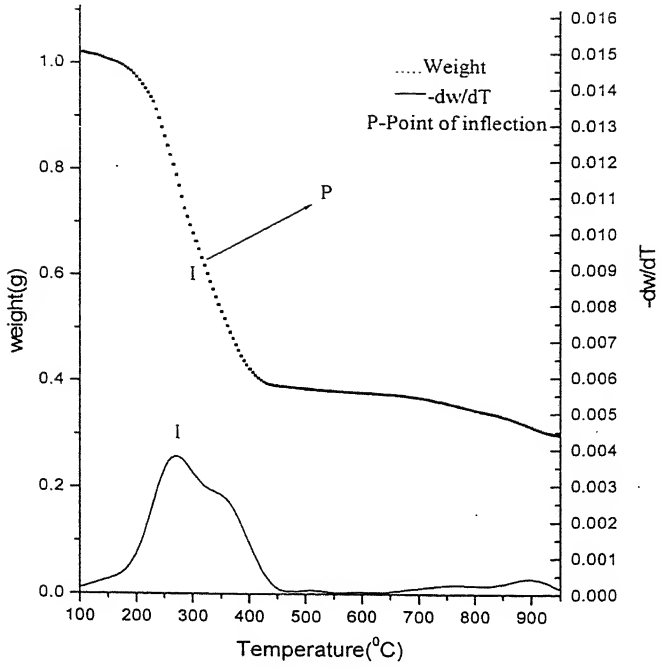

Fig.3.1 (g): Weight versus Temperature and –dw/dT versus Temperature plot for $Ba_xSr_{1-x}Fe_{0.8}Co_{0.2}O_{3-\delta}$ for x=1.0

Table 3.1 Parameters for $Ba_xSr_{1-x}Fe_{0.8}Co_{0.2}O_{3-\delta}$($0 \leq x \leq 1$)with initial mass of 1 g in each case derived from the TG curves

Barium content(x)	0				0.2				0.4			0.5	0.6			0.8			1.0	
Peak Value of Temperature associated with the peak(^{0}C)	225	360	540	730	240	380	600	810	225	395	750	270	240	370	790	230	380	740	270	900
Commulatative weight loss (mg)	150	320	560	670	130	450	680	750	210	580	800	350	120	540	800	100	600	750	220	700
Rate of change of weight with temperature (mg/^{0}C)	2.8	1.7	0.7	0.5	1.9	3.8	0.5	0.5	4.2	2.9	0.5	5	3.2	5.0	0.5	3.5	4.8	0.5	3.8	0.5
Stability: temperature range (^{0}C)	>900				>900				450-650 and > 850			450-650 and > 900	450-650 and > 820			450-650 and > 850			450-650 and > 900	

3.2 Phase evaluation

XRD pattern of pure sample together with a standard aluminum sample recorded with CuKα radiation is shown in fig 3.2.The diffraction peaks of aluminum are marked and used as a reference to calibrate the system and make corrections in values of the diffraction peaks of $Ba_xSr_{1-x}Fe_{0.8}Co_{0.2}O_{3-\delta}$ ($0 \leq x \leq 1$) compounds. The 2θ values, interplanar (d) spacing, and relative intensities of various diffraction peaks with their respective Miller indices are given in Table 3.2. It can be seen that all the compounds have nearly similar XRD patterns (except strontium free system, i.e., x=1). These compounds contain mainly the cubic perovskite type phase with another cubic phase in small quantity (as its peaks are weaker). But the cubic perovskite structure is well preserved throughout. It implies that the partial substitution of strontium with barium ion gets totally adjusted in the $SrFe_{0.8}Co_{0.2}O_{3-\delta}$ unit cell.

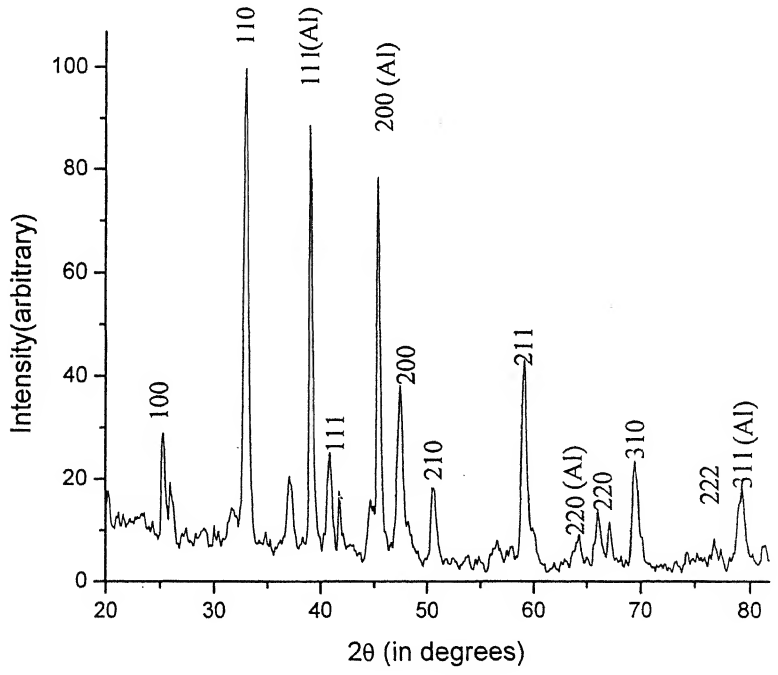

Fig.3.2: (a) XRD pattern of $Ba_xSr_{1-x}Fe_{0.8}Co_{0.2}O_{3-\delta}$ for x=0

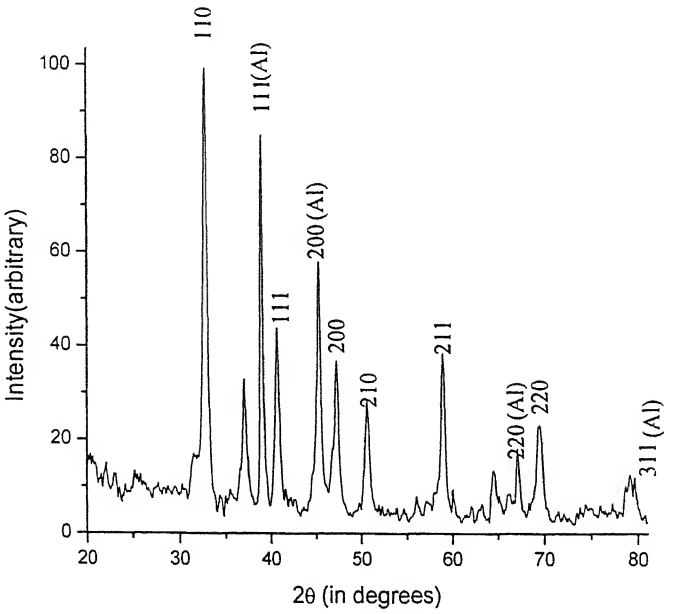

Fig.3.2: (b) XRD pattern of $Ba_xSr_{1-x}Fe_{0.8}Co_{0.2}O_{3-\delta}$ for x=0.2

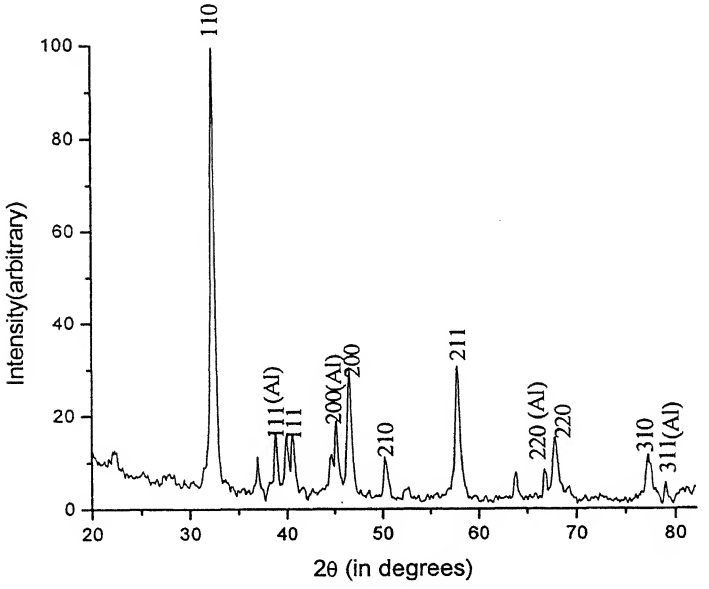

Fig.3.2: (c) XRD pattern of $Ba_xSr_{1-x}Fe_{0.8}Co_{0.2}O_{3-\delta}$ for x=0.4

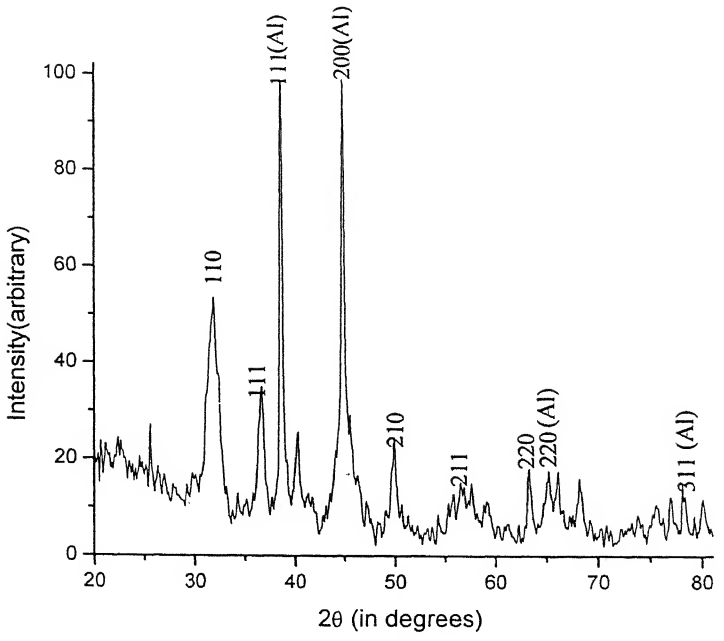

Fig.3.2: (d) XRD pattern of $Ba_xSr_{1-x}Fe_{0.8}Co_{0.2}O_{3-\delta}$ for x=0.5

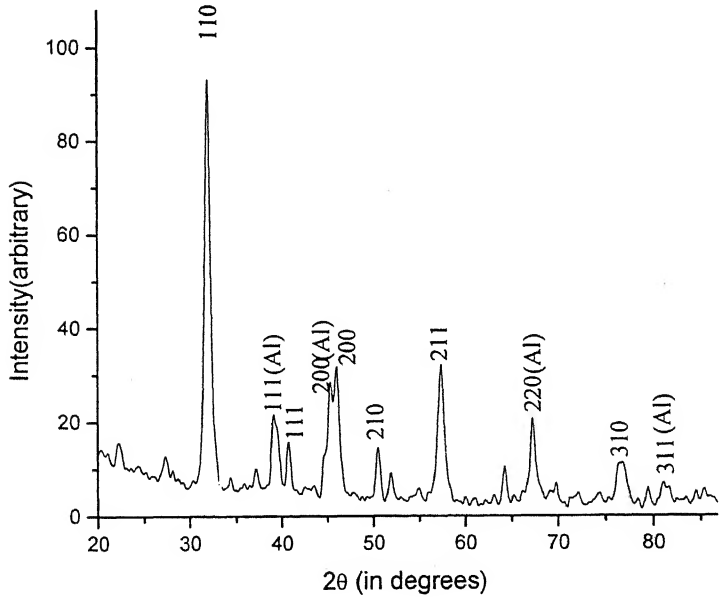

Fig.3.2: (e) XRD pattern of $Ba_xSr_{1-x}Fe_{0.8}Co_{0.2}O_{3-\delta}$ for x=0.6

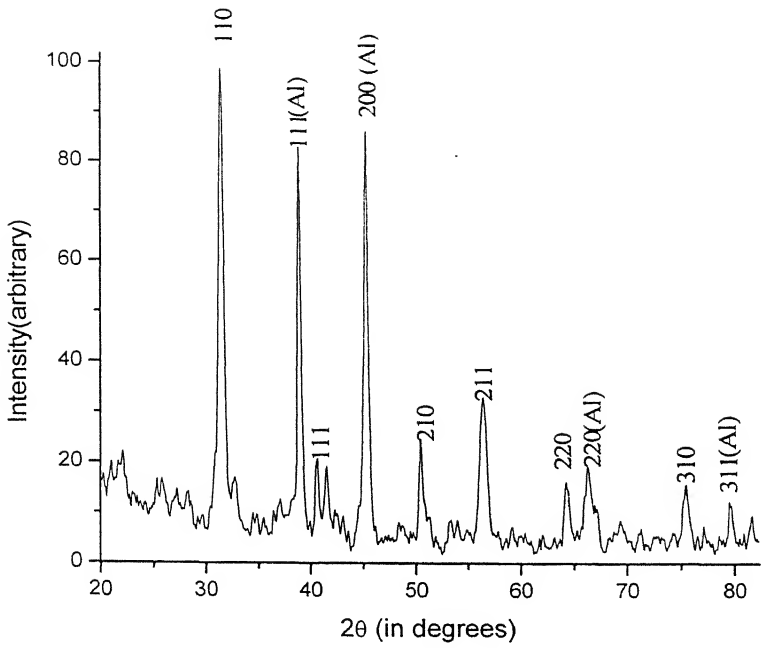

Fig.3.2: (f) XRD pattern of $Ba_xSr_{1-x}Fe_{0.8}Co_{0.2}O_{3-\delta}$ for x=0.8

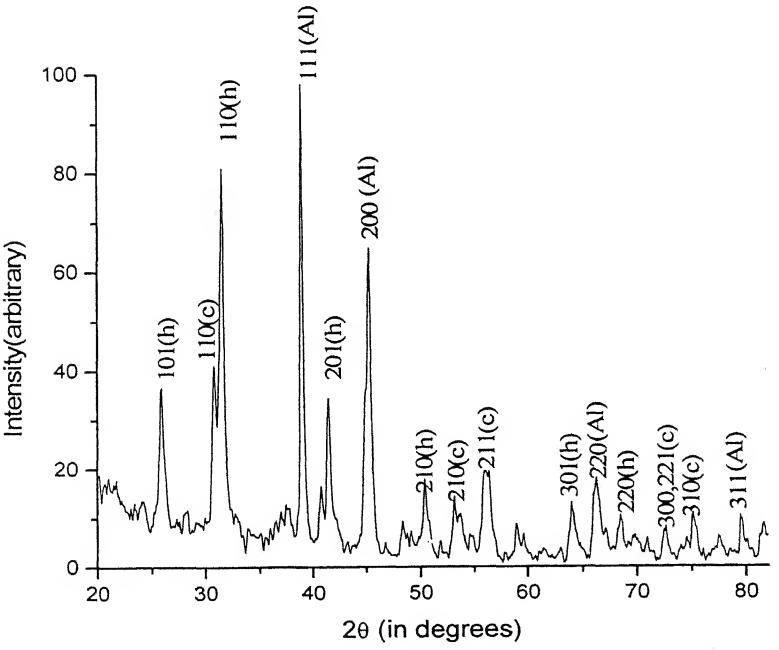

Fig.3.2: (g) XRD pattern of $Ba_xSr_{1-x}Fe_{0.8}Co_{0.2}O_{3-\delta}$ for x=1.0

Table 3.2: 2θ's, interplanar spacings and intensities of various peaks observed in XRD of $Ba_xSr_{1-x}Fe_{0.8}Co_{0.2}O_{3-\delta}$

X=0.0	2θ(°)	24.955	32.515	36.535	38.505	40.225	44.695	46.705	49.745	58.195	68.41	75.58	78.09	--	--
	Intensity	28.91	99.1	20.2	87.78	25.54	77.59	38.76	17.91	44.09	23.80	8.38	19.85	--	--
	d-values(Å)	3.554	2.745	2.452	2.332	2.236	2.023	1.941	1.829	1.583	1.371	1.258	1.224	--	--
	hkl	100	110	?	111(Al)	111	200(Al)	200	210	211	220	222	310	--	--
X=0.2	2θ(°)	32.475	36.655	38.505	40.215	44.695	46.645	49.865	58.045	65.985	68.275	78.215	--	--	--
	Intensity	100	33.2	85.34	44.42	56.82	37.03	28.22	36.99	17.22	23.19	12.57	--	--	--
	d-values(Å)	2.757	2.454	2.34	2.245	2.029	1.949	1.83	1.59	1.417	1.374	1.223	--	--	--
	hkl	110	?	111(Al)	111	200(Al)	200	210	211	220(Al)	220	311(Al)	--	--	--
X=0.4	2θ(°)	32.115	36.66	38.505	39.585	44.745	46.075	49.765	57.135	65.985	67.015	76.305	78.025	--	--
	Intensity	99.8	11.97	16.81	15.62	19.39	31.49	10.25	31.11	8.1	15.73	12.04	5.65	--	--
	d-values(Å)	2.785	2.45	2.337	2.275	2.024	1.969	1.831	1.611	1.415	1.396	1.248	1.224	--	--
	hkl	110	?	111(Al)	111	200(Al)	200	210	211	220(Al)	220	310	311(Al)	--	--
X=0.5	2θ(°)	31.715	34.165	38.505	40.22	41.205	44.745	46.21	49.785	56.425	57.59	63.23	65.065	68.105	78.085
	Intensity	52.18	34.85	100	24.39	12.32	96.33	16.40	24.51	15.5	15.04	18.54	16.35	14.52	11.12
	d-values(Å)	2.816	2.457	2.334	2.242	2.188	2.023	1.965	1.829	1.629	1.6	1.47	1.432	1.376	1.223
	hkl	110	111	111(Al)	?	?	200(Al)	?	210	211	?	220	220(Al)	?	311(Al)
X=0.6	2θ(°)	21.955	31.555	36.79	38.505	40.31	44.625	45.305	50.985	56.415	66.105	75.355	78.005	--	--
	Intensity	15.81	100	11.62	21.39	17.98	31.84	33.63	10.15	34.26	22.76	11.32	6.92	--	--
	d-values(Å)	4.013	2.819	2.44	2.323	2.23	2.022	1.994	1.785	1.626	1.45	1.258	1.222	--	--
	hkl	?	110	?	111(Al)	111	200(Al)	200	210	211	220(Al)	310	311(Al)	--	--
X=0.8	2θ(°)	22.065	31.235	38.505	40.10	44.695	49.775	55.51	63.22	65.235	74.165	78.215	--	--	--
	Intensity	22.79	100	80.56	20.25	86.18	24.81	33.38	16.12	20.25	16.1	11.54	--	--	--
	d-values(Å)	4.04	2.869	2.342	2.249	2.03	1.834	1.66	1.47	1.431	1.28	1.223	--	--	--
	hkl	?	110	111(Al)	111	200(Al)	210	211	220	220(Al)	310	311(Al)	--	--	--
X=1.0	2θ(°)	25.725	31.235	37.185	38.505	41.225	44.645	49.66	52.39	55.17	62.98	65.135	67.37	73.76	78.115
	Intensity	36.69	80.04	12.5	91.14	17.7	64.07	18.09	13.41	18.77	12.44	18.58	10.32	11.18	9.6
	d-values(Å)	3.459	2.86	2.416	2.336	2.242	2.028	1.836	1.746	1.665	1.475	1.431	1.39	1.285	1.223
	hkl	101	110	111	111(Al)	201	200(Al)	210	210	211	301	220(Al)	220	310	311(Al)

Fig.3.2.1 shows the schematic diagram of the ideal cubic perovskite structure in which A-cations occupy corners, B-cation lies at the cell centre and O^{2-} ions sit at the face centred positions. Each ion in the unit cell may be assumed to be of spherical shape. When the barium ion enters into the unit cell of $SrFe_{0.8}Co_{0.2}O_{3-\delta}$ and occupies the interstitial sites, there are three possible tetrahedral positions as shown in fig 3.2.1(b-d); i.e., within (a) the Sr1-O1-O2-O3,(b) the B-O1-O2-O3, and (c) Sr1-Sr2-O1-O3 tetrahedron , respectively.

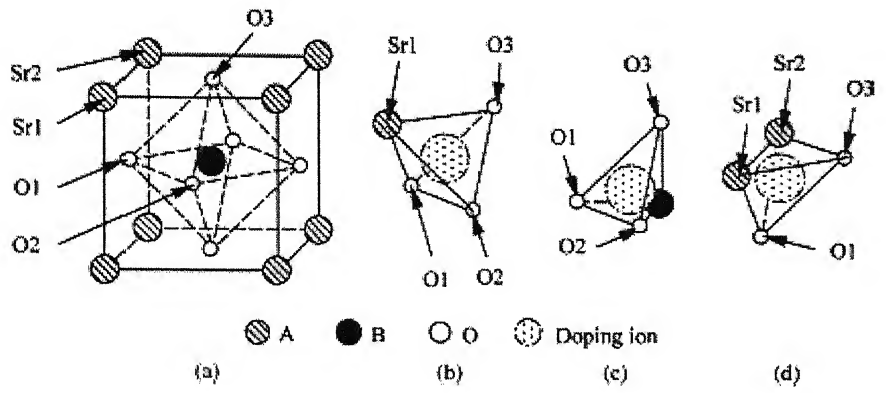

Fig.3.2.1 schematic diagram of (a) ideal ABO_3 -type perovskite structure, and (b, c and d) possible tetrahedral positions 1, 2 and 3 for Ba^{2+} ion on entering the $SrFe_{0.8}Co_{0.2}O_{3-\delta}$ unit cell.

The maximum radii of the sphere which can fit into the tetrahedral positions should be 0.263, 0.204 and 0.492 Å for positions depicted in fig.3.2.1 b, c and d, respectively. Thus, the largest sphere of radius 0.492 Å can enter into the $SrFe_{0.8}Co_{0.2}O_{3-\delta}$ without distorting the unit cell. The ionic radius of Ba^{2+} is 1.34 Å, which is much larger than 0.492 Å. The insertion of barium ion should therefore result in an overall expansion or distortion of the unit cell. Obviously, these sites seem to be unfavorable for the Ba^{2+} ions. Considering the size of various ions ($r_{Co2+} = 0.72\,Å, r_{Fe2+} = 0.74\,Å, r_{O2-} = 1.32\,Å, r_{Sr2+} = 1.12\,Å, r_{Ba2+} = 1.34\,Å$), the most probable locations for Ba^{2+} ions are Sr^{2+} sites only. Since the Ba^{2+} ion is slightly larger than Sr^{2+}, it is expected that the unit cell of the substituted compounds exhibit a minor increase in size. Needless to say that the tolerance factor (t) for the synthesized compounds takes the value in the range 0.92 to 0.997.

The analysis of XRD patterns of $Ba_xSr_{1-x}Fe_{0.8}Co_{0.2}O_{3-\delta}$ ($0 \leq x \leq 1$) reveals all (except x=1.0) to possess perovskite type cubic structure with the lattice parameter in the range 3.888 ± 0.004 Å to 4.052 ± 0.004 Å for x = 0 to 0.8 (Table 3.3). The increase of lattice parameter with rise in barium content can be attributed to the larger size of barium in comparison to strontium. Fig 3.2.2 shows the variation of lattice parameter as a function of barium content.

Table 3.3: Crystal structure and lattice parameter of $Ba_xSr_{1-x}Fe_{0.8}Co_{0.2}O_{3-\delta}$ ($0 \leq x \leq 1$) compounds

Barium content(x)	0	0.2	0.4	0.5	0.6	0.8	1.0
Crystal structure	cubic	cubic	cubic	cubic	cubic	cubic	hexagonal
Lattice parameter ± 0.004(Å)	3.888	3.889	3.944	3.955	4.008	4.052	a= 5.889, c=4.653
Known lattice parameter(Å)	3.863[68]	-	-	3.979[68]	-	-	a=5.590, c=4.820[69]

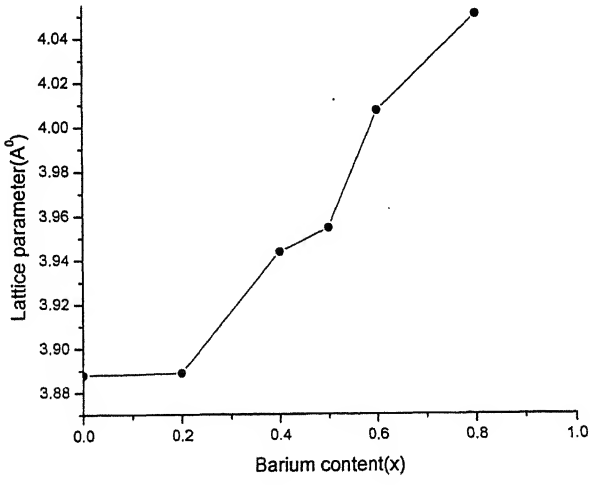

Fig.3.2.2: Barium content versus lattice parameter

The lattice parameter values agree well with the pervious reports on $SrFe_{0.8}Co_{0.2}O_{3-\delta}$ and $Ba_{0.5}Sr_{0.5}Fe_{0.8}Co_{0.2}O_{3-\delta}$ systems, the value being 3.863 Å and 3.979 Å , respectively [68]. For $BaFe_{0.8}Co_{0.2}O_{3-\delta}$ compound (i.e., strontium free system), the crystal structure is hexagonal with lattice parameters a = 5.889 Å ± 0.004 Å, c = 4.653 Å ± 0.004Å (Table 3.3), consistent with the pure $BaFeO_{3-\delta}$ compound which crystallizes in hexagonal structure with a = 5.590 Å, c = 4.820 Å [69]. It may be mentioned that XRD pattern contain some extra weak peaks corresponding to a cubic perovskite phase with lattice parameter a ~ 4.074 Å as well. This implies that a small quantity of cubic perovskite phase co-exists with the main hexagonal phase.

3.3 Magnetic Measurements:

The magnetization vs magnetic field curves of $Ba_xSr_{1-x}Fe_{0.8}Co_{0.2}O_{3-\delta}$ ($0 \leq x \leq 1$) at room temperature are shown in fig 3.3.1.Their saturation magnetization (M_s),coercivity and curie temperature values are summarized in Table 3.4. Clearly there is decrease of magnetization with increase of the barium content in $Ba_xSr_{1-x}Fe_{0.8}Co_{0.2}O_{3-\delta}$ system. Also the saturation magnetization is invariably lower than that of $SrFe_{0.8}Co_{0.2}O_{3-\delta}$ (i.e., barium free compound). It suggests that barium substitution is somehow contributing to lowering of overall magnetization. Further, with increase in barium content there is decrease in magnetic saturation with widening of the hysteresis loop (i.e., increase in the coercivities value).The highest value of coercivity is found for $BaFe_{0.8}Co_{0.2}O_{3-\delta}$ compound which exhibits hexagonal structure.

The decrease in the value of saturation magnetization is somewhat deceptive as the cobalt-iron content itself decreases with increase of barium in $Ba_xSr_{1-x}Fe_{0.8}Co_{0.2}O_{3-\delta}$ (molecular weight being continuously increasing). Therefore the saturation magnetization is expected to decrease as magnetic species are effectively reduced with progressive substitution of strontium with barium. Considering the effect of decrease in content of cobalt-iron alone, the saturation magnetization should decrease by factor α, given by

$$\alpha = \frac{\text{Molecular Weight of } Sr\,Fe_{0.8}Co_{0.2}O_3}{\text{Molecular Weight of } Ba_xSr_{1-x}Fe_{0.8}Co_{0.2}O_3}$$

Table 3.3 list values of saturation magnetization after correction for the effective decrease of cobalt-iron content. Accordingly, decrease in saturation magnetization should have been more than found experimentally. The possible reason could be change in the environment of magnetic species with increased substitution of strontium by a slightly larger size barium (ionic radii of Sr^{2+} and Ba^{2+} being 1.12Å and 1.34Å ,respectively).Still the variation is too small to infer about the role of Ba^{2+} with certainty.

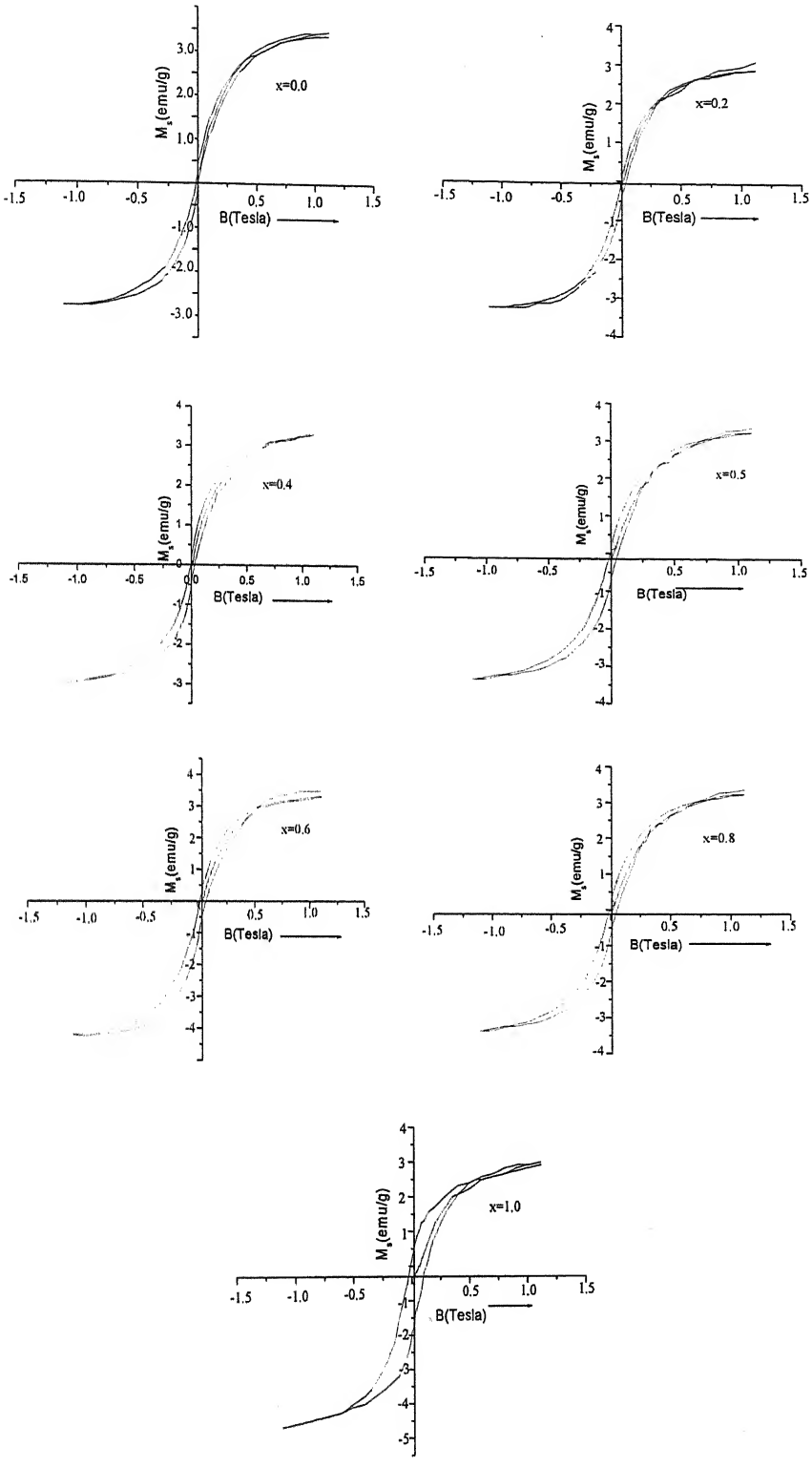

Fig 3.3.1: Hysteresis curves of $Ba_xSr_{1-x}Fe_{0.8}Co_{0.2}O_{3-\delta}$ ($0 \leq x \leq 1$)

Table 3.4: The values of magnetization (M_s), coercivity (H_c), curie temperature, and factor (α) of $Ba_xSr_{1-x}Fe_{0.8}Co_{0.2}O_{3-\delta}$ compound in the range x=0 to 1.

Barium content(x)	0.0	0.2	0.4	0.5	0.6	0.8	1.0
Saturation Magnetization (emu/g)	3.31	3.27	3.18	3.09	2.96	2.82	2.71
Coercivity H_c(× 10^{-4} Tesla)	49	53	71	79	98	125	150
α	1	0.95	0.91	0.89	0.87	0.83	0.79
Saturation Magnetization (emu/g) *	3.31	3.14	3.01	2.95	2.88	2.75	2.61
Curie Temperature(^{0}C)	575			600			

* expected change due to Co-Fe content variation in per gram of the sample

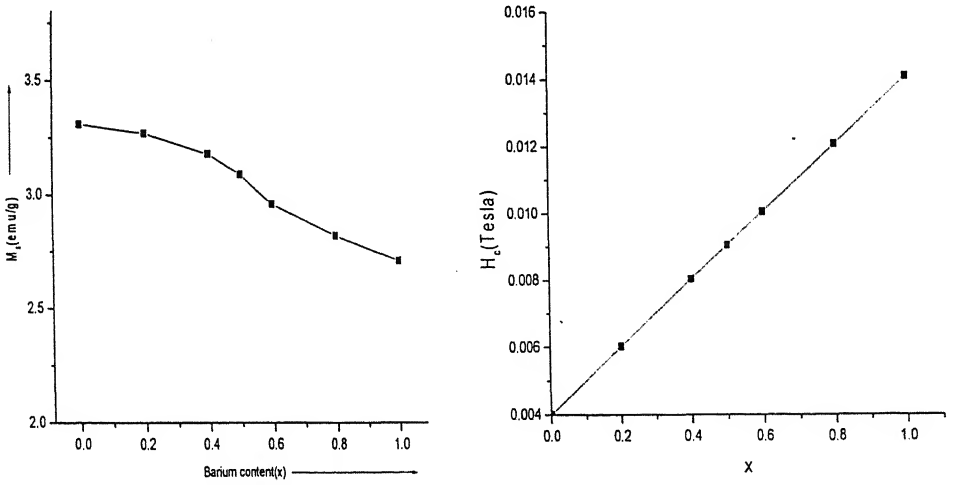

Fig 3.3.2: Hysteresis parameters versus compositions

The magnetization versus temperature (T) curves for the composition x=0 and x=0.5 at a fixed magnetic field of 0.05T are shown in fig 3.3.3. The magnetization value first decreases continuously but slowly with increase of temperature upto a point beyond which the change is somewhat abrupt. Curie temperature (T_c) values determined by the intersection of tangent drawn at the point of highest slope in the magnetization versus temperature curve with abscissa are 575^0C and 600^0C for x=0 and x=0.5, respectively. This result is indicative of better magnetic stability of $Ba_{0.5}Sr_{0.5}Fe_{0.8}Co_{0.2}O_{3-\delta}$ compound in comparison to $SrFe_{0.8}Co_{0.2}O_{3-\delta}$ compound.

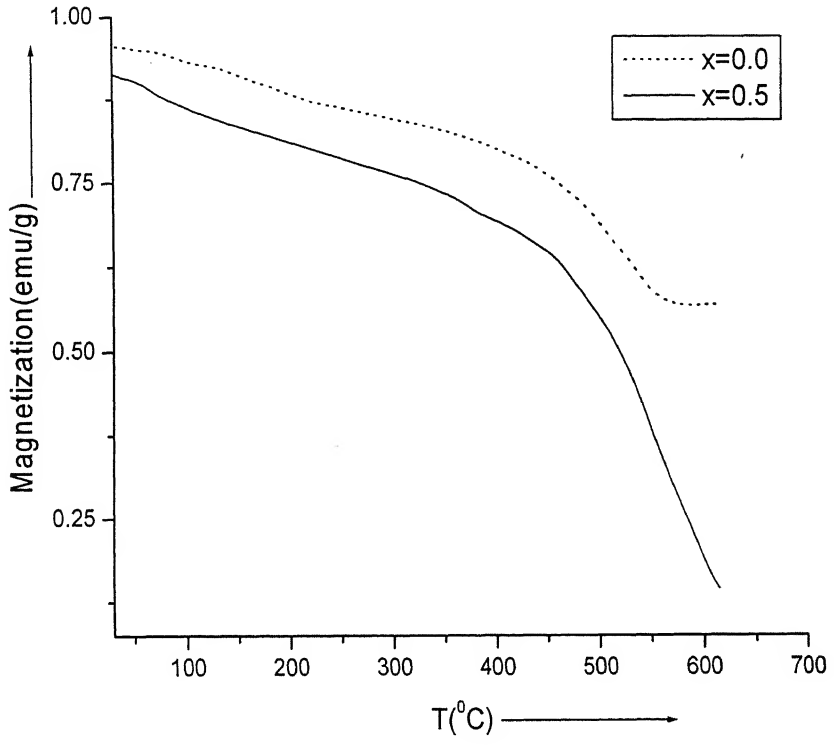

Fig 3.3.3: Magnetization versus Temperature

3.4 Oxygen Temperature-programmed desorption:

In O_2-TPD experiment the oxygen releases from compound with rise in temperature via creation of oxygen vacancies by reduction of metal ions from high valance state to lower valance state. The O_2-TPD profiles of $Ba_xSr_{1-x}Fe_{0.8}Co_{0.2}O_{3-\delta}$ (for x=0 and x=0.5) are shown in fig 3.4 and corresponding peak temperatures and areas under the curve are listed in Table 3.5.The points that emerge from these results are:

(a) the shifting of peaks towards higher temperature with barium insertion , i.e., leading to improved stability.

(b) oxidation of Co^{3+} and Fe^{3+} to higher valance state Co^{4+} and Fe^{4+} is effectively facilitated with the introduction of barium.

(c) area under the peak increases with barium substitution implying thereby that $Ba_{0.5}Sr_{0.5}Fe_{0.8}Co_{0.2}O_{3-\delta}$ is a better membrane for oxygen separation than $SrFe_{0.8}Co_{0.2}O_{3-\delta}$. The optimum working temperatures for these membranes turns out to be 850^0C and 915^0C respectively.

(d) for x=0.5, another broad peak appear around 300-450^0C.This implies partial substitution of strontium by barium influences the bonding energy of metal-ion and oxygen.

XRD pattern of the ceramic membranes recorded after O_2-TPD experiments are shown in fig 3.5.Their analysis reveal suppression of diffraction peaks and decrease of lattice parameter by 1-1.5%.It is expected as desorption leads to creation of oxygen vacancies in the membranes.

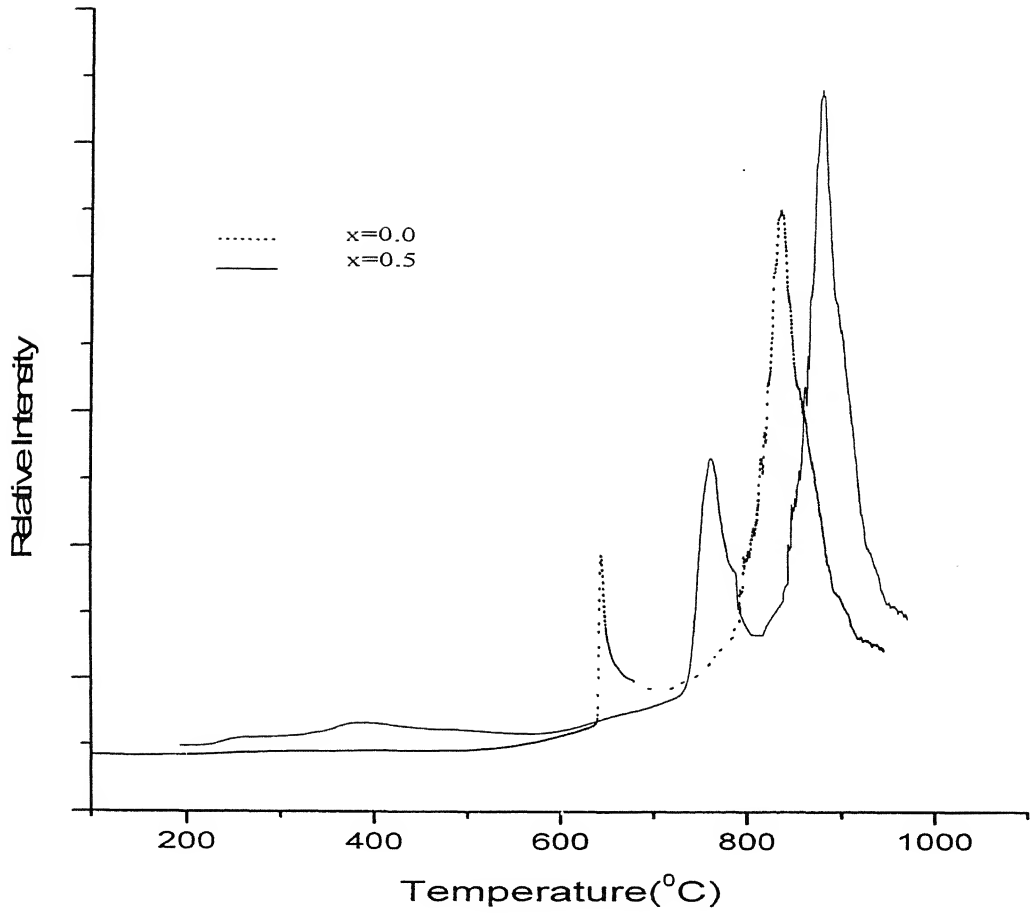

Fig.3.4.O_2-TPD curves of $Ba_xSr_{1-x}Fe_{0.8}Co_{0.2}O_{3-\delta}$ for x=0 and 0.5

Table 3.5: Parameters of O_2-TPD profile:

Barium content(x)	0.0		0.5	
Peak temperatures(^{0}C)	650	850	760	915
Area under the peak in arbitrary unit	8.247×10^7	9.615×10^8	2.36×10^8	3.360×10^9

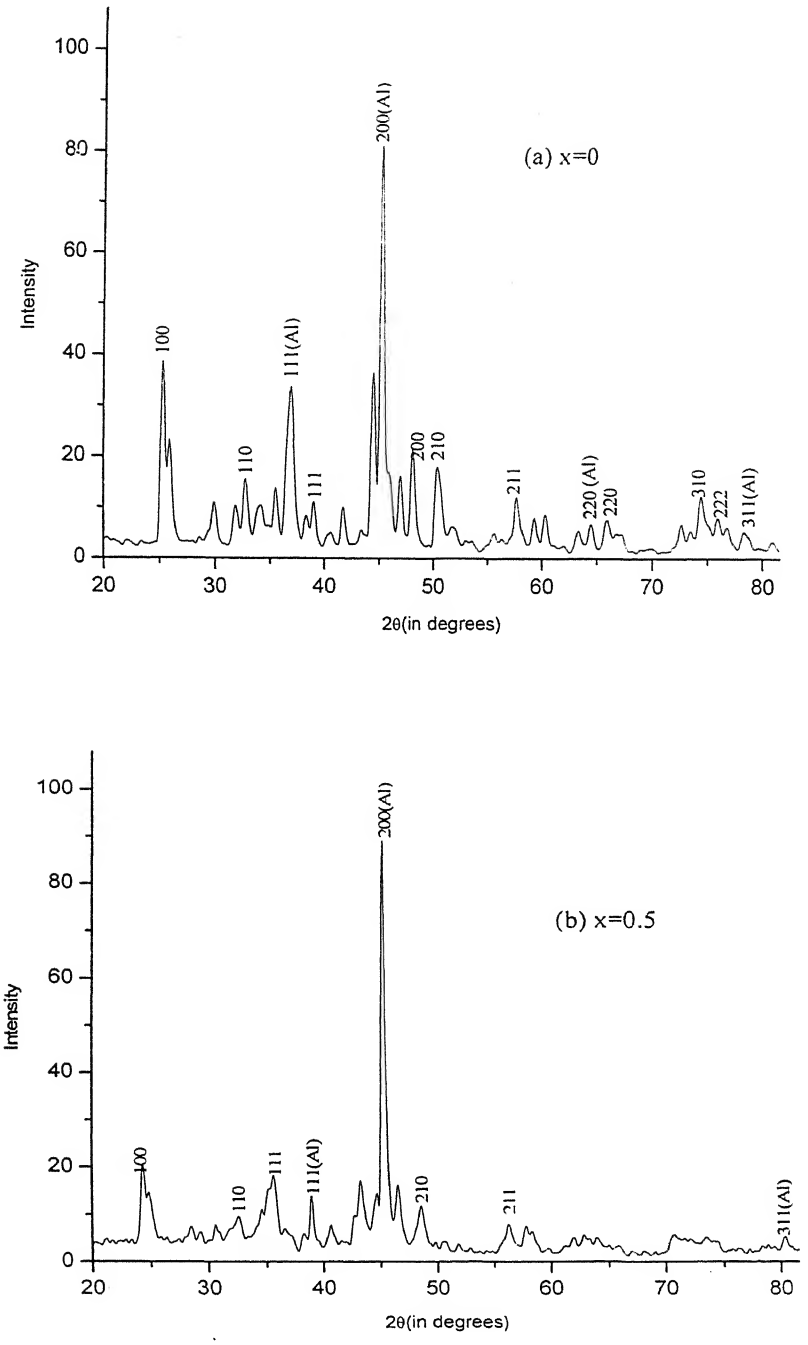

Fig.3.5: XRD patterns of $Ba_xSr_{1-x}Fe_{0.8}Co_{0.2}O_{3-\delta}$ compounds after O_2-TPD experiment for (a) x=0, and (b) x=0.5

4. Conclusions

1. A series of ceramic membranes of compositions $Ba_xSr_{1-x}Fe_{0.8}Co_{0.2}O_{3-\delta}$ ($0 \leq x \leq 1$; in the interval of x=0.2) can be synthesized successfully by a combined citrate-EDTA complexing method.

2. The membranes of all composition are quite stable at 900-950^{0}C. Barium insertion makes the compound stable even at lower temperature range of 450-650^{0}C.

3. $Ba_xSr_{1-x}Fe_{0.8}Co_{0.2}O_{3-\delta}$ compounds exhibit a perovskite type cubic structure with progressively larger lattice parameter as the barium content increases from x=0 to x=0.8; the lattice parameter being in the range 3.888 Å - 4.052 Å. $BaFe_{0.8}Co_{0.2}O_{3-\delta}$ compound depicts an hexagonal structure with lattice parameters a = 5.889 Å, c = 4.653 Å(The accuracy being ± 0.004 Å).

4. Magnetization value decreases while coercivity value increases with increase in barium content. Further, the Curie temperature of $SrFe_{0.8}Co_{0.2}O_{3-\delta}$ and $Ba_{0.5}Sr_{0.5}Fe_{0.8}Co_{0.2}O_{3-\delta}$ compound is 575^0 and 600^{0}C, respectively.

5. The optimum working temperature of the membranes for oxygen separation is above 850^0 and 915^{0}C for compositions $SrFe_{0.8}Co_{0.2}O_{3-\delta}$ and $Ba_{0.5}Sr_{0.5}Fe_{0.8}Co_{0.2}O_{3-\delta}$, respectively.

5. References

[1] H.J.M. Bouwmeester, A.J. Burbbraaf, *"Dense ceramic membranes for oxygen separation"*, in: A.J. Burggraaf, L.Cot (Eds.), Fundamentals of Inorganic membrane Science and Technology, chapter 10, Elsevier, Amsterdam 1996.

[2] B.K.Flandermeyer, M.M.Nasrallah, D.M. Sparlin and H.U.Anderson, in: "Transport *in Nonstiochiometric compounds* ", eds.V.Stubican and G.Sinkovich (Plenum, New York, 1985) p.17.

[3] J.H. Kuo, H.U.Anderson and D.M.Sparlin, J.Solid State Chem. 83(1989) 52; 87(1990) 55.

[4] T.Nakamura, G.Petzow and L.Gauckler, Mat.Res. Bull. 14(1979) 649.

[5] J.Mizusaki, M. Yoshihiro, S.Yamauchi and K.Fueki, Solid State Chem. 58(1985) 257.

[6] J.Mizusaki, S. Yamauchi, K.Fueki and A.I.Ishikawa, Solid State Ionics 12 (1984) 119.

[7] B.C.H.Steele,Mat.Sci.Eng. B 13 (1992) 79.

[8] C.Y.Tsai, Y.H.ma.W.R. Moser, A.G.Dixon, "*Simulation Of Nonisothermal Catalytic Membrane Reactor For Methane Partial Oxidation To Syngas*",in: Y.H.Ma(Ed.), Proceedings of 3rd International Conference on Inorganic Membranes, Worcester,July 10-14, 1994,p.271.

[9] C.Y. Tsai, A.G. Dixon,W.R.Moser,Y.H. Ma, "*Dense perovskite membrane reactors for partial oxidation of methane to syngas*",AIChE J.43(1997) 2741.

[10] S.Pei, M.S.Kleefisch, T.P.Kobylinski, K.Faber, C.A.Udovich, V.Zhang-Mccoy,B.Dabrowski,U.Balachandran,R.L.Mieville,R.B.Poeppel,"*Failure mechanism of ceramic membrane reactors in partial oxidation of methane to synthesis gas*",Catal. Lett.30 (1995) 201.

[11] U.Balachandran, J.T.Dusk, R.L.Mieville, R.B.Poeppel, M.S.Kleefisch, S.Pei, T.P.Kobylinski, C.A.Udovich, A.C. Bose, "*Dense Ceramic membranes for partial oxidation of methane to syngas*" , Appl.Catal.A:Gen.133 (1995) 19.

[12] U.Balachandran,J.T.Dusk,P.S.Maiya,B.Ma,R.L.Mieville,M.S.Kleefisch,C.A.Udovich, "*Ceramic membrane reactor for converting methane to syngas Catal*".Today 36(1997) 265

[13] J.E.ten Elshof, B.A.Van Hassel, H.J.M.Bouwmeester, "*Activation of methane using solid oxide membrane*", Catal.Today 25(1995) 397.

[14] J.E.ten Elshof,H.J.M.Bouwmeester,H.Verweij,"*Oxidative coupling of methane in a mixed-conducting perovskite membrane reactor*",Appl.Catal.A : Gen.130(1995) 195.

[15] Y.S.Lin,Y.Zeng,"*Catalytic properties of oxygen semipermeable perovskite type ceramic membrane materials for oxidative coupling of methane*",J.Catal.164(1996) 220.

[16] J. Zaman and A. Chakma, "*Inorganic membrane reactors*," *J. Membr. Sci.*, **92** (1994) 1-28.

[17]] G. Saracco and V. Specchia, "*Catalytic inorganic-membrane reactors: Present experience and future opportunities*," *Catal. Rev.-Sci. Eng.*, **36** (1994) 305-384.

[18] D. Eng and M. Stoukides, "*Catalytic and electrocatalytic methane oxidation with solid oxide membranes*," *Catal. Rev.-Sci. Eng.*, **33** (1991) 375-412.

[19] C.G. Vayenas, S. Bebelis, I.V. Yentekakis and H.G. Luntz, "*Non-faradaic electrochemical modification of catalytic activity*," *Catal. Today*, **11** (1992) 303-442.

[20] P. Shuk, H.-D. Wiemhöfer, U. Guth, W. Göpel and M. Greenblatt, "*Oxide ion conducting solid electrolytes based on Bi_2O_3*," *Solid State Ionics*, **89** (1996) 179-196.

[21] S. Dou, C.R. Masson and P.D. Pacey, "*Mechanism of oxygen permeation through limestabilized zirconia*," *J. Electrochem. Soc.*, **132** (1985) 1843-1849

[22] H.J.M. Bouwmeester, H. Kruidhof, A.J. Burggraaf and P.J. Gellings, "*Oxygen semipermeability of erbia-stabilized bismuth oxide*," *Solid State Ionics*, **53-56** (1992) 460-468.

[23] B. Calès and J.F. Baumard, "*Mixed conduction and defect structure of ZrO_2-CeO_2-Y_2O_3 solid solutions*," *J. Electrochem. Soc.*, **131** (1984) 2407-2413.

[24] G.Z. Cao, X.Q. Liu, H.W. Brinkman, K.J. de Vries and A.J. Burggraaf, "*Mixed conduction and oxygen permeation of ZrO_2-$Tb_2O_{3.5}$-Y_2O_3 solid solutions*," in: *Science and Technology of Zirconia V*, ed. S.P.S. Badwal, M.J. Bannister and R.H.J. Bannink, Technomic Publishing, Lancaster, 1993, p. 576-583.

[25] I.C. Vinke, B.A. Boukamp, K.J. de Vries and A.J. Burggraaf, "*Mixed conductivity in terbiastabilized bismuth oxide*," *Solid State Ionics*, **57** (1992) 91-98.

[26] Y. Teraoka, H.-M. Zhang, S. Furukawa and N. Yamazoe, "*Oxygen permeation through perovskite-type oxides*," *Chem. Let.*, (1985) 1743-1746.

[27] J. Mizusaki, "*Nonstoichiometry, diffusion, and electrical properties of perovskite-type oxide electrode materials*," *Solid State Ionics*, **52** (1992) 79-91.

[28] H.U. Anderson, "*Review of p-type doped perovskite materials for SOFC and other applications*," *Solid State Ionics*, **52** (1992) 33-41.

[29] Y. Teraoka, T. Nobunaga and N. Yamazoe, "*Effect of cation substitution on the oxygen semipermeability of perovskite-type oxides*," *Chem. Let.*, (1988) 503-506.

[30] Y. Teraoka, T. Nobunaga, K. Okamoto, N. Miura and N. Yamazoe, "*Influence of constituent metal cations in substituted $LaCoO_3$ on mixed conductivity and oxygen permeability*," *Solid State Ionics*, **48** (1991) 207-212.

[31] S. Carter, A. Selcuk, R.J. Chater, J. Kajda, J.A. Kilner and B.C.H. Steele, "*Oxygen transport in selected nonstoichiometric perovskite-type oxides*," *Solid State Ionics*, **53-56** (1992) 597-605.

[32] T. Ishigaki, S. Yamauchi, K. Kishio, J. Mizusaki and K. Fueki, "*Diffusion of oxide ion vacancies in perovskite-type oxides*," *J. Solid State Chem.*, **73** (1988) 179-187.

[33] L. Qiu, T.H. Lee, L.-M. Liu, Y.L. Yang and A.J. Jacobson, "*Oxygen permeation studies of $SrCo_{0.8}Fe_{0.2}O_{3-\delta}$*," *Solid State Ionics*, **76** (1995) 321-329.

[34] H. Kruidhof, H.J.M. Bouwmeester, R.H.E. van Doorn and A.J. Burggraaf, "*Influence of order-disorder transitions on oxygen permeability through selected nonstoichiometric perovskite-type oxides*,"*Solid State Ionics*,,**63-65**(1993) 816-822.

[35] V.V. Kharton, E.N. Naumovich and A.V. Nikolaev, "*Oxide ion and electron conjugate diffusion in perovskite-like $SrCo_{1-x}M_xO_{3-\delta}$(M=Cr,Cu; x=0,0.5)*," *Solid State Phenom.*, **39-40** (1994) 147-152.

[36] V.V. Kharton, E.N. Naumovich, A.V. Nikolaev and V.V. Samokhval, "*Development of mixed conductive materials for high-temperature electrochemical oxygen membranes*," in: Proc. 17th Risø Intl. Symp. on Mat. Sci.: *High Temperature Electrochemistry: Ceramics and Metals*, ed. F.W. Poulsen, N. Bonanos, S. Linderoth, M. Mogensen and B. Zachau-Christiansen, Risø National Laboratory, Roskilde, Denmark, 1996, p. 301-306.

[37] N. Itoh, T. Kato, K. Uchida and K. Haraya, "*Preparation of pore-free disks of $La_{1-x}Sr_xCoO_3$ mixed conductors and its oxygen permeability*," *J. Membr. Sci.*, **92** (1994) 239-246.

[38] R.H.E. van Doorn, H. Kruidhof, H.J.M. Bouwmeester and A.J. Burggraaf, "*Oxygen permeability of strontium-doped $LaCoO_{3-\delta}$*," in: *Materials Research Society Symposium Proceedings, Vol. 369, Solid State Ionics IV*, ed. G.-A. Nazri, J.-M. Taracson and M.S. Schreiber, Materials Research Society, Pittsburgh, PA, 1995, p. 373-382.

[39] V.V. Kharton, E.N. Naumovich, A.A. Vecher and A.V. Nikolaev, "*Oxide ion conduction in solid solutions $Ln_{1-x}Sr_xCoO_{3-\delta}$(Ln=La, Pr, Nd)*," *J. Solid State Chem.*, **120** (1995) 128-136.

[40] H.W. Brinkman, H. Kruidhof and A.J. Burggraaf, "*Mixed conducting yttrium-barium-cobaltoxide for high oxygen permeation*," *Solid State Ionics*, **68** (1994) 173-176.

[41] J.W. Stevenson, T.R. Armstrong, R.D. Carneim, L.R. Pederson and W.J. Weber, "*Electrochemical properties of mixed conducting perovskites $La_{1-x}M_xCo_{1-y}Fe_yO_3$ (M=Sr, Ba, Ca)*," *J. Electrochem. Soc.*, **143** (1996) 2722-2729.

[42] N. Miura, Y. Okamoto, J. Tamaki, K. Morinaga and N. Yamazoe, "*Oxygen semipermeability of mixed-conductive oxide thick-film prepared by slip casting*," *Solid State Ionics*, **79** (1995) 195-200.

[43] B.A. van Hassel, J.E. ten Elshof and H.J.M. Bouwmeester, "*Oxygen permeation flux through $La_{1-y}Sr_yO_3$ limited by carbon monoxide oxidation rate*," *Appl. Cat. A*, **119** (1994) 279-291.

[44] N. Sakai, T. Horita, H. Yokokawa, M. Dokiya and T. Kawada, "*Oxygen permeation measurement of $La_{1-x}Ca_xCrO_{3-\delta}$ by using an electrochemical method*," *Solid State Ionics*, **86- 88** (1996) 1273-1278.

[45] T. Kawada, T. Horita, N. Sakai, H. Yokokawa and M. Dokiya, "*Experimental determination of oxygen permeation flux through bulk and grain boundary of $La_{0.7}Ca_{0.3}CrO_3$*," *Solid State Ionics*, **79** (1995) 201-207.

[46] H. Iwahara, T. Esaka and T. Mangahara, "*Mixed conduction and oxygen permeation in the substituted oxides for $CaTiO_3$*," *J. Appl. Electrochem.*, **18** (1988) 173-177.

[47] T.J. Mazanec, T.L. Cable and J.G. Frye, jr., "*Electrocatalytic cells for chemical reaction*," *Solid State Ionics*, **53-56** (1992) 111-118.

[48] Y. Shen, M. Liu, D. Taylor, S. Bolagopal, A. Joshi and K. Krist, "*Mixed ionic-electronic conductors based on Bi-Y-O-Ag metal-ceramic system*," Proc. 2nd Intl. Symp. on *Ionic and mixed conducting ceramics*, ed. T.A. Ramanarayanan, W.L. Worrell and H.L. Tuller, Proc. vol. 94-12, The Electrochemical Society, Pennington, NJ, 1994, p. 574-597.

[49] C.S. Chen, H. Kruidhof, H.J.M. Bouwmeester, H. Verweij and A.J. Burggraaf, "*Oxygen permeation through oxygen ion oxide-noble metal dual phase composites*," *Solid State Ionics*, **86-88** (1996) 569-572.

[50] H.J.M. Bouwmeester, "*Dense ceramic membranes for oxygen separation," in: CRC Handbook Solid State Chemistry,* ed. P.J. Gellings and H.J.M. Bouwmeester, CRC Press, Boca Raton, 1996, p. 481-553.

[51] H. Nagamoto, K. Hayashi and H. Inoue, "*Methane oxidation by oxygen transported through solid electrolyte*," *J. Catal.*, **126** (1990) 671-673.

[52] J. Lede, F. Lapicque, J. Villermaux, B. Cales, A. Ounalli, J.F. Baumard and A.M. Anthony, "*Production of hydrogen by direct thermal decomposition of water: preliminary investigations*," *Int. J. Hydrogen Energy*, **7** (1982) 939-950.

[53] B. Calès and J.F. Baumard, "*Production of hydrogen by direct thermal decomposition of water with the aid of a semipermeable membrane*," *High Temperatures-High Pressures*, **14** (1982) 681-686.

[54] Y. Nigara and B. Cales, "*Production of carbon monoxide by direct thermal splitting of carbon dioxide at high temperature*," *Bull. Chem. Soc. Jpn.*, **59** (1986) 1997-2002.

[55] N. Itoh, M.A. Sanchez C., W.-C. Xu, K. Haraya and M. Hongo, "*Application of a membrane reactor system to thermal decomposition of CO_2*," *J. Membr. Sci.*, **77** (1993) 245-253.

[56] R. Di Cosimo, J.D. Burrington and R.K. Graselli, "*Oxidative dehydrodimerization of propylene over a Bi_2O_3-La_2O_3 oxide ion-conductive catalyst*," *J. Catal.*, **102** (1986) 234-239.

[57] T. Hibino, T. Sato, K. Ushiki and Y. Kuwahara, "*Membrane reactor for oxidative coupling of CH_4 with an oxide ion-electron hole conductor*," *J. Chem. Soc. Faraday Trans.*, **91** (1995) 4419-4422.

[58] S. Pei, M.S. Kleefisch, T.P. Kobylinski, J. Faber, C. Udovich, V. Zhang-McCoy, B. Dabrowski, U. Balachandran, R.L. Mieville and R.B. Poeppel, "*Failure mechanisms of ceramic membrane reactors in partial oxidation of methane to synthesis gas*," *Catal. Let.*, **30** (1995) 201-212.

[59] U. Balachandran, J.T. Dusek, S.M. Sweeney, R.B. Poeppel, R.L. Mieville, P.S. Maiya, M.S. Kleefisch, S. Pei, T.P. Kobylinski, C. Udovich and A.C. Bose, "*Methane to syngas via ceramic membranes*," *Am. Cer. Soc. Bull.*, **74** (1995) 71-75.

[60] T. Nozaki, O. Yamazaki, K. Omata and K. Fujimoto, "*Selective oxidative coupling of methane with membrane reactor,*" *Chem. Eng. Sci.*, **47** (1992) 2945-2950.

[61] J.E. ten Elshof, unpublished work.

[62] C.-Y. Tsai, Y.H. Ma, W.R. Moser and A.G. Dixon, "*Modeling and simulation of a nonisothermal catalytic membrane reactor*," *Chem. Eng. Commun.*, **134** (1995) 107-132

[63] H. Schmalzried, *Solid state reactions*, 2nd ed., Verlag Chemie, Weinheim-Deerfield Beach- Basel, 1981.

[64] C. Wagner, "*Beitrag zur Theorie des Anlaufvorgangs*," *Z. Phys. Chem.*, **21** (1933) 25-41.

[65] C.S. Chen, Chapter 2 in *Fine grained zirconia-metal dual phase composites*, Thesis, University of Twente, Enschede, the Netherlands, 1994.

[66] J. Nowotny and J.B. Wagner, jr., "*Influence of the surface on the equilibration kinetics of nonstoichiometric oxides*," *Oxid. Met.*, **15** (1981) 169-190.

[67] Z. Adamczyk and J. Nowotny, "*Effect of the surface on gas/solid equilibration kinetics on nonstoichiometric compounds*," *Solid State Phenom. - Diffusion and Defect Data*, **15&16** (1991) 285-336.

[68] Zongping Shao,Weishen Yang,You Cong,Hui Dong,Jianhua Tong,Guoxing Xiong, "*Investigation of the permeation behavior and stability of a* $Ba_{0.5}Sr_{0.5}C0_{0.8}Fe_{0.8}O_{3-\delta}$ ",Journal of membrane science,172(2000)177-188.

[69] Powder diffraction file 10-245.

[70]] Liang Tan,Li Yang,Xuehong Gu,Wanqin Jin,Lixiong Zhang,Nanping Xu," *Influence of the size of doping ion on phase stability and oxygen permeability of* $SrFe_{0.8}Co_{0.2}O_{3-\delta}$ *oxide*", Journal of membrane science, 230(2004) 21-27.

[71] Y.Teraoka,H.M. Zhang,N.Yamazoe,"*Oxygen-sorption properties of perovskite-type* $La_{1-x}Sr_xCo_{1-y}Fe_yO_{3-\delta}$ ",Chem.Lett 165(1985)1367-1370.

[72] S.Pei,M.S. Kleefisch, T.P. Kobylinski , J.Faber, C.A.Udovich, V.ZhangMcCoy, B.Dabrowski, U.Balachandran, R.L. Mieville, R.B. Poeppel, "*Failure mechanism of ceramic membrane reactors in partial oxidation of methane to synthesis gas*",Catal.Lett. 30(1995) 201-212.

[73] C.Y. Tsai,A.G. Dixon, Yi Hua Ma, W.R. Mose, M.R. Pascucci, "*Dense perovskite* $La_{1-x}A'_xFe_{1-y}Co_yO_{3-\delta}$*(A'= Ba,Sr,Ca) membrane synthesis,application and characterization*",J. Am.Ceram.Soc, 86(1998) 1437-1444.

[74] T.Daniels "*Thermal Analysis" chapter-3* "BIP chemicals Ltd,Warley,Worcestershire England.